https://doi.org/10.1016/j.compstruct.2021.115001

Compressive and Transverse Shear Behaviour of Novel FRP-UHPC Hybrid Bars

Jun-Jie Zeng[a,b*], Yu-Yi Ye[a], Wai-Meng Quach[b], Guan Lin[c], Yan Zhuge[d], Jie-Kai Zhou[a]

[a] School of Civil and Transportation Engineering, Guangdong University of Technology, Guangzhou 510006, China.
[b] Department of Civil and Environmental Engineering, University of Macau, Macau, China.
[c] Department of Civil and Environmental Engineering, The Hong Kong Polytechnic University, Hong Kong, China.
[d] UniSA STEM, University of South Australia, South Australia 5095 Australia.
*Corresponding author. E-mail: jjzeng@gdut.edu.cn (Jun-Jie Zeng)

Abstract: Fibre-reinforced polymer (FRP) bars have become increasingly popular as internal reinforcement in reinforced concrete (RC) structures due to their excellent corrosion resistance. However, the compressive strength of FRP bars is generally much inferior to their tensile strength due to fibre micro-buckling under compression, and their transverse shear performance is much inferior to that of steel bars with the same diameter. To this end, a novel form of steel-free hybrid bars, which consist of an outer FRP confining tube, a central FRP bar and a layer of ultra-high performance concrete (UHPC) (without steel fibres) in the annular space between them (referred to as FRP-UHPC hybrid bars), have been proposed. In this study, compressive and transverse shear behaviour of FRP-UHPC hybrid bars have been investigated via experimentation. The key test variables include fibre winding angles of the FRP tube, fibre types of the FRP tube, the FRP tube thickness and the diameter of the central FRP bar. The test results confirm the validation of the novel hybrid bars: i) the compressive stress-strain curves of hybrid bars exhibit a ductile behaviour with a strain hardening segment, and the compressive behaviour of the central FRP bar in hybrid bars is superior to that of FRP bars in isolation; ii) the stress-strain response of hybrid bars can be designed to meet an elastic-plastic response with a post-yielding strain-hardening response; and iii) the transverse shear performance of hybrid bars is much better than that of FRP bars in isolation due to the contribution of FRP-confined UHPC section.

Keywords: fibre-reinforced polymer (FRP) bar; ultra-high performance concrete (UHPC), hybrid bar; confinement; axial compressive behaviour; transverse shear behaviour.

1. Introduction

Steel corrosion is the major cause for the deterioration of conventional steel reinforced concrete (RC) structures, especially for those structures located in marine and other aggressive environments. To eliminate steel corrosion, the use of fibre-reinforced polymer (FRP) bars instead of steel bars as internal reinforcement in RC structures has been proposed and studied by some researchers [1-5]. Existing studies have shown that FRP bars are expected to become a cost-effective and environmentally-friendly alternative to steel bars in RC structures due to their merits such as excellent corrosion resistance, high strength-weight ratio and electromagnetic transparency [6-8]. However, FRP bars as longitudinal reinforcement in concrete members are inevitable to resist compressive stresses. They are easily damaged under compression due to fibre micro-buckling, unless they are well supported by a proper confining device. As a result, their compressive strength is known to be much lower than their tensile strength [9-11]. ACI 440.1R-15 [12] does not recommend the use of FRP bars as longitudinal reinforcement in compressed members while CSA S806-12 (R2017) [13] neglects the compressive resistance and stiffness of FRP longitudinal reinforcement in the compression zone in design. In such cases, FRP bars predominantly serve as tensile reinforcement in RC structures. It should be mentioned that although the compressive strength of FRP bars can be neglected in design, inevitable considerable compressive stresses raised by special loadings (e.g., seismic loading) in FRP bars may lead to degradation in their tensile strength. The degradation in the tensile strength of FRP bars is unacceptable. This is because the tensile strength of concrete is generally negligible in the design of RC structures and tensile stresses can only be resisted by FRP bars in FRP-RC structures. Therefore, the way to improve the compressive strength of FRP bars becomes a concern in the field of FRP-RC structures.

In order to enhance the material properties of FRP bars (e.g., low elastic modulus and brittle failure manner) or protect the steel from corrosion in aggressive environments, steel-FRP composite bars (SFCB) which comprise an outer FRP layer and a core steel rod (or steel wires) [14-18], and hybrid FRP (HFRP) bars which consist of different types of fibres [19-21] have been proposed. Wu et al. [15,16] studied the mechanical properties of SFCBs under uniaxial and cyclic tensile loads. It was found that SFCBs can exhibit an elastic-plastic stress-strain behaviour with a high elastic modulus and a good tensile ductility due to the contribution from the core steel rod. You et al. [20] developed a novel form of HFRP rods by using carbon and E-glass fibres and the results showed that the ultimate strains of the hybrid rods can be increased by up to 33% compared to the non-hybrid carbon FRP rods. Additionally, HFRP bars (carbon/basalt fibres) have better transverse shear strength than the basalt FRP bars, as reported by Protchenko et al. [21]. It is obvious that these investigations on SFCBs or HFRP bars mainly focus on improving the tensile and shear properties of FRP bars. The failure of HFRP bars caused by fibre micro-buckling is still inevitable. SFCBs may also have corrosion problems due to the presence of the steel bar. Particularly, RC structures reinforced with SFCBs are not applicable to situations where the use of steel reinforcement must be avoided, including hospital buildings with magnetic resonance imagining (MRI) facilities.

Against the above background, Teng et al. [22] recently developed a novel form of steel-free hybrid bars. The hybrid bar consists of a central FRP bar, an outer FRP confining tube and a layer of ultra-high performance concrete (UHPC) (without steel fibres) in the annular space between them (referred to as FRP-UHPC hybrid bars or simply hybrid bars herein), as shown in Fig. 1. In such a hybrid bar, the central FRP bar is well confined by the FRP-confined UHPC so that both fibre micro-buckling and overall buckling are prevented or delayed, and the compressive capacity of the central FRP bar is expected to be fully exploited. UHPC is an advanced cementitious material which has a dense micro-structure and unique merits such as high-strength (a compressive strength of over 150 MPa [23-26]), high-ductility and superior durability [27,28]. As the strength of UHPC is generally much higher than the normal-strength concrete, UHPC generally fails in a brittle manner. Therefore, FRP confinement has been introduced for UHPC, and the strength and deformation capacity of UHPC can be substantially enhanced by FRP confinement [29-32]. In addition, UHPC has a higher elastic modulus than that of the normal-strength concrete, and the elastic modulus of UHPC is close to that of the FRP bar under compression (around 40 GPa). This leads to excellent compatibility of the components in hybrid bars. As the central FRP bar in hybrid bars can remain intact even after the UHPC has experienced crushing failure, the hybrid bars exhibit a ductile stress-strain response with a linear first segment and a strain-hardening second segment. Additionally, hybrid bars can resist both tensile and compressive stresses effectively, with the tensile stresses being resisted mainly by the central FRP bar and the compressive stresses being resisted by both the central FRP bar and the UHPC layer.

Teng et al. [22] have conducted preliminary axial compressive tests on hybrid bars. The results indicated that hybrid bars had an excellent performance under compression, and both FRP bar buckling and fibre micro-buckling were prevented. It was also found that the stress-strain response of hybrid bars can be designed to meet performance needs (e.g., to exhibit an elastic-plastic response like that of steel or a strong post-yielding strain-hardening response). As mentioned earlier, the conventional FRP-concrete members (Fig. 2a) may fail in a very brittle manner in compression because of the linear brittle behavior of FRP bars. By using hybrid bars as the longitudinal reinforcement in RC columns (Fig. 2b), the load-deformation response of hybrid bar RC columns is expected to be superior to that of the FRP bar RC columns (Fig. 2c).

So far, there have been only limited studies on the fundamental mechanical properties of FRP-UHPC hybrid bars (e.g., [22]). These existing studies on hybrid bars failed to clarify the effects of some key parameters such as winding angle of fibres in the confining FRP tube. On the other hand, the RC structural members are inevitably subjected to transverse shear forces, and the design of shear capacity of RC members reinforced with hybrid bars is an essential requirement. Although existing standards or guidelines (e.g., [33,34]) generally neglect the shear capacity of longitudinal bars in the design shear resistance, it cannot be denied that the dowel action of longitudinal bars is beneficial and the understanding on the transverse shear response of longitudinal bars is important especially in members without shear reinforcement. As the confining FRP tube and the UHPC layer may also enhance the transverse shear performance of FRP bars, studies on the transverse shear performance of hybrid bars are necessary to validate the contribution of confining FRP tubes and UHPC layers in resisting the shear force. For hybrid bars to be subsequently utilized in construction, further experimental investigations are needed to explore the effects of various parameters on the compressive and transverse shear behaviour of hybrid bars. To this end, this paper presents a first-ever experimental study on the transverse shear behaviour of novel FRP-UHPC hybrid bars. The effect of various parameters on the axial compressive behaviour of hybrid bars has also been carefully investigated. The key test variables include fibre winding angles of the FRP tube (i.e., filament orientation angle with respect to the longitudinal axis of the FRP tube), fibre types of the FRP tube, the FRP tube thickness and the diameter of the central FRP bar. In addition to hybrid bars, UHPC-filled FRP tube specimens which have been studied to some extent [29-32], were also prepared as control group and tested under axial compression and transverse shear loading to investigate the effect of the central FRP bar on the mechanical performance of hybrid bars. Therefore, a comprehensive study on mechanical properties of hybrid bars, including compression and transverse shear tests of hybrid bars, are conducted in this study to gain an in-depth understanding of hybrid bars.

2. Material Properties

2.1 Ultra-high-performance concrete

The UHPC was manufactured in the laboratory by utilizing the mixing methodology reported in Teng et al. [28]. The raw materials used to produce UHPC, included: i) the P•II 52.5R Portland cement; ii) the silica fume with a silica content of 93%; iii) the natural river sand with the maximum particle size less than 2.36 mm; iv) the 20-40 mesh and 70-140 mesh dried quartz powder (half each by weight, and mesh number is the number of holes in one square inch of the sieve); v) the polycarboxylate-based super-plasticizer with a solid content of 20%; and vi) the local tap water sourced from Guangzhou, China, as shown in Table 1. Note that the composite specimens (including hybrid bars and UHPC-filled FRP tubes) were cast in two different batches of UHPC materials, and for each batch of UHPC, the actual compressive properties were determined from the average test results of three standard cylinders (50 × 100 mm) tested right before the start of testing of the composite specimens, as per ASTM standards [35,36]. The compressive properties of each batch of UHPC are given in Table 2.

It should be mentioned that the two batches of UHPC were produced at different ambient temperature (the ambient temperature when casting the Batch 2 UHPC (12±4℃) was lower than that when casting the Batch 1 UHPC (31±4℃)), but their mix proportions (Table 1), raw materials, mixing methodology and curing condition were identical. The workability of the Batch 2 UHPC was inferior to that of the Batch 1 UHPC due to the sensitivity of the super-plasticizer to the temperature. Based on free mini-slump spread tests were conducted as per ASTM C1856/C1856M-17 [33], the average slump spread diameters for the Batch 1 UHPC (240 mm) were larger than that of the Batch 2 UHPC (200 mm). The low compressive strength of the Batch 2 concrete is thus resulted from their poor workability.

2.2 FRP tube

Two types of FRP tubes, including carbon FRP (CFRP) and glass FRP (GFRP) tubes, were used in the current study. All FRP tubes had an internal diameter of 50 mm. The CFRP tubes were manufactured in the laboratory by manually winding a unidirectional high tensile strength carbon fibre sheet impregnated with epoxy resin around a small-size polyvinyl chloride (PVC) tube (i.e., the wet-layup process). An overlapping zone with a 50-mm length was adopted in each FRP tube to avoid the premature FRP debonding failure. The fibres of FRP tubes were oriented only in the hoop direction (i.e., fibre winding angle at ±90° with respect to the tube longitudinal axis) so that they served predominantly as a confining device. Material properties of the CFRP were obtained via standard coupon tensile tests in accordance with ASTM D3039-15 [37]. The coupon test results showed that the average elastic modulus of the CFRP was 227.3 GPa based on a nominal thickness of 0.167 mm/ply of the carbon fibre sheet, while the average rupture strain was 1.60%.

The GFRP tubes used in this experiment were small-scale filament-wound FRP tubes provided by Guangdong SUNNY FRP CO., Ltd. The fibre winding angle of GFRP tubes included ±45°, ±60° and ±80°. Despite having the same number of layers, GFRP tubes with different fibre winding angles had different actual average thickness. As a result, the material properties of GFRP tubes were based on their actual average thickness (see the second column of Table 3). A split disk test method was adopted based on the ASTM D2290-19 [38]. For each type of small GFRP tube, five rings with a width of 25 mm were prepared and tested. A total of six hoop strain gauges were installed on the outer surface of each specimen at opposite locations for strains in the tubes (see Fig. 3a). All FRP rings were loaded by a 100-kN-capacity universal test machine with a displacement-control rate of 2 mm/min. The typical failure modes of FRP rings are shown in Fig. 3b, where FRP rings showed a combined failure mode with both fibre ruptures and fibre delamination. The hoop stress-strain curves are plotted in Fig. 3c, in which the hoop stresses were obtained by dividing the applied tensile force by two times the cross-sectional area of the ring cross-section and the strains were averaged from the four hoop strain gauges away from the gaps (Fig. 5a) to eliminate any effects from the local bending at the gaps. The results illustrate that a lower fibre winding angle leads to a lower stiffness and higher nonlinear behaviour (e.g., GFRP tubes with a fibre winding angle at ±45° have a significant nonlinearity) (Fig. 3c). This is because the deformation of small GFRP tubes was induced by both the stretching of the fibre and the change of fibre winding angle during the test. The elastic modulus of the nonlinear FRP was taken as the secant stiffness at the peak point. Results from the tensile tests of small GFRP rings are summarized in Table 3.

Compression tests were also conducted on nine four-layer GFRP rings (including three duplicate samples for each group GFRP tube) to obtain the compressive material properties of FRP tubes according to GB/T 5350-2005 [39]. All the FRP rings, cut from the same batch of FRP tubes used for hybrid bars and their reference specimens (i.e., UHPC-filled small FRP tube), had a total height of 60 mm (including the test length of 30 mm). Four axial strain gauges at 90 degree apart and two hoop strain gauges at 180 degree apart were arranged at the mid-height of FRP rings. FRP rings were loaded axially at a rate of 0.5 mm/min. FRP rings exhibited a typical local buckling failure mode, accompanied with the splitting of resin (Fig. 4a). The compressive stress-strain curves are shown in Fig. 4b and key test results of GFRP rings in compression are given in Table 4. The results show that GFRP rings with a fibre winding angle of ±60° have the highest compressive strength (slightly larger than those with a fibre winding angle of ±45°), followed by those with a fibre winding angles of ±45° or ±80°. This is because the actual average thickness of the GFRP rings with a fibre winding angle of ±45° was larger than that of the GFRP rings with a fibre winding angle of ±60° (see Table 3).

2.3 FRP bars

Two types of GFRP bars were used in this study, including a ribbed bar with a nominal diameter of 25 mm and a sand-coated bar with a nominal diameter of 16 mm. The tensile properties of FRP bars were obtained via GB/T 30022-2013 [40] (see Fig. 5a). Figure 5c shows the tensile stress-strain curves, and test results are summarized in Table 5. It was found that both the tensile strength and the modulus of elasticity of the FRP bar with a nominal diameter of 16 mm were higher than those of the FRP bar with a nominal diameter of 25 mm.

To further understand the compressive properties of FRP bars, ten bare FRP bars (i.e., five duplicated specimens for each group) with an unsupported length-to-diameter ratio of 4 were also prepared and tested under axial compression. A set of hollow steel caps was specially designed according to the method of Alajarmeh et al. [11], and was filled with high strength gypsum to provide confinement to the ends of the FRP bar (see Fig. 5). It should be noted that the height of steel caps was 30 mm; and thus the total length of the sample with a nominal diameter of 25 mm was 160 mm, and that of the sample with a nominal diameter of 16 mm was 124 mm. All samples were subjected to axial compression tests with a displacement-control rate of 1.5 mm/min (see Fig. 5a). As shown in Fig. 5b, GFRP bars with a nominal diameter of 25 mm experienced a splitting failure, with many vertical cracks being developed along the unsupported length; while those with a nominal diameter of 16 mm experienced a shear failure near the end, accompanied with fibre delamination at the end. Figure 5c shows the compressive stress-strain curves, and test results are summarized in Table 5. The average compressive elastic modulus of GFRP bars with the nominal diameters of 25 mm and 16 mm were 41.0 GPa and 47.6 GPa, respectively; which were equal to 99% and 103% of the tensile elastic modulus of the corresponding GFRP straight bars, respectively. Note that the tensile and compressive elastic modulus of FRP bars was determined from two points on the stress-strain curve of the FRP bar before the peak axial stress: Point 1 with an axial strain of 0.005% and Point 2 with an axial strain corresponding to 40% of peak axial stress. The higher compressive elastic modulus than tensile elastic modulus for smaller diameter bars was probably due to the full engagement of all fibres within the cross-section of the bar [11]. It was also found that the compressive strengths of these two types of GFRP bars were much smaller than their tensile strengths, especially for the GFRP bars with a nominal diameter of 25mm.

3. Compression Tests and Results

3.1 Specimens design and test set-up

A total of 51 small-size circular hybrid bar specimens and reference specimens (i.e., UHPC-filled small FRP tube specimens) were fabricated and tested. All the testing specimens had a diameter of 50 mm (i.e., the internal diameter of the prefabricated FRP tube) and a height of 150 mm. The effects of fibre winding orientation angles of the FRP tube (e.g., ±45°, ±60° and ±80°), fibre types of the FRP tube (e.g., GFRP and CFRP), the FRP tube thickness and the diameter of central FRP bar (e.g., FRP bar with a nominal diameter of 16 mm or 25 mm) were investigated. Three nominally identical specimens were tested for each group. As shown in Table 6, for ease of reference, each specimen was labeled with five sets of symbols separated from each other by a character "-". The first symbol represents the number of batches ("S1" for the first batch, "S2" for the second batch). The second symbol indicates the FRP type ("G" for GFRP, "C" for CFRP) with the corresponding digit representing the number of FRP layers. The third symbol indicates the fibre winding angle of FRP tubes. The fourth symbol represents the diameter of the central FRP bar (where "0" indicates UHPC-filled small FRP tube specimens). The last symbol ("1", "2" or "3") is used to distinguish the three duplicate specimens in each group. For instance, "S1-G4-45-25-1" refers to the first hybrid bar specimen confined with a four-layer GFRP tube with a fibre winding angle at ±45° and reinforced with a central FRP bar with a nominal diameter of 25 mm in the first batch.

The preparation of hybrid bars is shown in Fig. 6. Firstly, the central FRP bar and outer FRP tube was fixed at the wooden laminate through adhesive. Fresh UHPC was then poured into the annular space between the central FRP bar and the outer FRP tube, during which a small vibrator was used to compact the UHPC. Prefabricated FRP tubes can be used as not only the outer confining material but also a mold for UHPC cylinders. All specimens were first cured at the room temperature in the water tank for 14 days, and they were then cured in the structural laboratory of Guangdong University of Technology for more than 14 days. The FRP tube had a length of 620 mm. The 620-mm-length specimen was cut into four 150-mm-length hybrid bar (or UHPC-filled FRP tube) specimens. Both ends of specimens were strengthened with a 2-ply CFRP sheet with a width of 12 mm to avoid the premature failure of FRP.

High strength gypsum was used to level the specimen ends to ensure uniform loading on the column cross-section (Fig. 7). All specimens were axially loaded on a hydraulic testing machine (with a maximum load of 4000 kN) with a displacement loading rate of 0.2 mm/min (Fig. 8). Two measurement methods were used to measure the axial deformation of the specimen: i) two linear variable displacement transducers (LVDTs) with an interval of 180° were installed to measure the full-height deformation of the specimen; and ii) four strain gauges with 20-mm gauge length were installed on the FRP tube to measure axial strains at the mid-height section. Other four strain gauges were installed to measure hoop strains in the FRP tubes. All the test results were logged simultaneously by an automatic data acquisition system.

3.2. Failure Modes

A complete failure of both hybrid bar specimens and UHPC-filled FRP tube reference specimens was caused by the rupture of the outer FRP tube at the mid-height region (see Fig. 9 for typical failure modes of specimens). Compared with the specimens produced from GFRP tubes, the specimens produced from CFRP tubes failed with a larger explosion sound. It was also found that the central FRP bar in hybrid bar specimens failed prior to the failure of the outer FRP tube, leading to a sudden decrease in the axial load. In comparison with specimens with a fibre winding angle at ±60° or ±80°, specimens with a fibre winding angle at ±45° had a greater deformation (see S1-G4-45-0-3 and S1-G4-45-25-1 in Figs. 9a and 9b). After the outer FRP tube was removed, it was witnessed that the UHPC core of UHPC-filled FRP tube was split into two parts and an obvious shear plane can be observed (see Fig. 9i). In the hybrid bars, the integrity of concrete was preserved except for the place where the FRP ruptured. As a result, the central FRP bar only had shear failure in a certain area (Fig. 9j).

3.3. Axial Stress-Strain Responses

The stress-strain curves (including axial stress-axial strain curves and axial stress-hoop strain curves) of UHPC-filled small GFRP tube reference specimens and hybrid bar specimens are shown in Figs. 10-12. The adopted axial stress was the average value of the axial load divided by the internal cross-sectional area of the outer FRP tube, and the axial contribution of FRP tubes was ignored in the current study due to their small axial stiffness [32]. The axial strains presented in this section were based on the data from the full-height LVDTs, and the hoop strains were obtained from the average readings of strain gauges located at the mid-height and on the outer surface of the FRP tube (strain gauges outside the overlapping zone for CFRP tubes). It should be noted that the termination point of each stress-strain curve corresponds to the rupture of outer FRP tube. However, some hoop strain gauges had failed before the FRP ruptured. In such a case, a straight line (i.e., dot dash line) with the same slope as that at the failure point was used to smoothly extend the axial strain-hoop strain curves until the measured FRP hoop rupture strain; and this will be discussed in the subsequent section. The values of the failure point of hoop strain gauges were also marked in the penultimate column of Table A1 in the Appendix. As the data recorded by full-height LVDTs included the displacement between the specimen and the loading plates of the machine, the average readings of axial strain gauges were used to correct the full-height LVDT data during the early loading stages (within the axial strain of around 0.004). The curves in each group are close to each other, as shown in Figs. 10-12, demonstrating a good test setup and a high reliability of the test results. It should be noted that the test results of specimen S2-G6-80-0-3 was not obtained due to unexpected breakdown of the loading machine.

As seen from Fig. 13a, the stress-strain behaviour of hybrid bar specimens can be generally characterized as a five-portion response: i) an elastic initial portion $[(0,0) \rightarrow (\varepsilon_{c1}, f'_{c1})]$; ii) stress fluctuation second portion $[(\varepsilon_{c1}, f'_{c1}) \rightarrow (\varepsilon_{c2}, f'_{c2})]$; iii) strain hardening third portion

$[(\varepsilon_{c2}, f'_{c2})$→$(\varepsilon_{c3}, f'_{c3})]$; iv) stress reduction fourth portion induced by failure of the central FRP bar $[(\varepsilon_{c3}, f'_{c3})$→$(\varepsilon_{c4}, f'_{c4})]$; and v) residual stress fifth portion $[(\varepsilon_{c4}, f'_{c4})$→$(\varepsilon_{cu}, f'_{cu})]$. At the elastic initial portion, the average axial stress increased approximately proportional to the axial strain (a small part of non-linearity can be seen at the final part of this elastic portion). After the axial strain approached the crushing strain of UHPC materials, the stress became unstable and fluctuated. This was caused by the brittleness of UHPC material and the micro gaps between the UHPC layer and the outer FRP tube [29-31], and the FRP confinement was not fully activated in this stage [32]. Depending on the confinement level of the outer FRP tube, the stresses in this portion (i.e., second portion) may have a descending or ascending trend (see Figs. 10a, 12a-12c). It was also found that the stress fluctuation of hybrid bars was less significant than that of UHPC-filled small FRP tube specimens due to the presence of central FRP bar (see each sub-figure in Fig. 11). Subsequently, the UHPC dilated and the passive confinement of the outer FRP tube was activated. The hybrid bars thus exhibited an obvious strain-hardening behaviour in the third portion. This strain-hardening portion ends when the failure of either the central FRP bar or the outer FRP tube happens, depending on the strain capacity of the outer FRP tube and the ultimate compressive strain of the central FRP bar. In general, the central GFRP bar failed earlier than the outer FRP tube at a specific axial deformation, accompanied with a sudden stress reduction. This is because the ultimate axial strain of FRP bars obtained from material tests is generally smaller than that of FRP-confined UHPC. The stress reduction and the corresponding axial strain in the fourth portion were associated with the level of confinement provided by the outer FRP tube (see Figs. 12a-12c). The larger the confining stress was, the smaller the stress reduction and the larger the value of ε_{c3} was. In the fifth portion, the hybrid bar specimens were subjected to residual stresses due to the effective confinement from the outer FRP tube although the central FRP bar had been damaged. The specimens finally failed by rupture of the outer FRP tube, accompanied with a substantial decrease in the axial load.

Unlike hybrid bar specimens, UHPC-filled small FRP tube specimens exhibited an obvious axial stress-strain relationship with three portions, as shown in Fig. 13b: i) an elastic initial portion $[(0, 0)$→$(\varepsilon_{c1}, f'_{c1})]$; ii) stress fluctuation second portion $[(\varepsilon_{c1}, f'_{c1})$→$(\varepsilon_{c2}, f'_{c2})]$; and iii) strain hardening third portion $[(\varepsilon_{c2}, f'_{c2})$→$(\varepsilon_{cu}, f'_{cu})]$. Similarly, the so-called second stress fluctuation portion was caused by the brittleness of UHPC materials and the confinement lag effect, as explained by Zeng's research group [32].

It is noted that in the present study, the first peak point ($\varepsilon_{c1}, f'_{c1}$), the first post-peak ravine point ($\varepsilon_{c2}, f'_{c2}$), the second peak point ($\varepsilon_{c3}, f'_{c3}$), the second post-peak ravine point ($\varepsilon_{c4}, f'_{c4}$) and the ultimate point (at FRP rupture) ($\varepsilon_{cu}, f'_{cu}$) are referred to as characteristic points. Table A1 summarizes the key data of these characteristic points for all specimens. FRP hoop rupture strain ($\varepsilon_{h,rup}$) is also given in Table A1. Some of the specimens did not exhibit a five-portion behavior and their characteristic points are not given (marked by 'N.A.') in Table A1. It is clearly shown that the average FRP hoop rupture strain is generally smaller than the FRP tensile strain, as reported by some other scholars [41,42]. This also indicates that the effect of reduced scale of FRP tubes has a little influence on the average strain efficiency factor of FRP.

3.4. Dilation Behaviour

The dilation behaviour of UHPC-filled small FRP tube and hybrid bar specimens was characterized by their axial strain-hoop strain relationship presented in Figs. 14-16. Overall, the axial strain-hoop strain curves of the three duplicated specimens are close to each other. As the hoop strains are terminated due to the premature failure of some hoop strain gauges, a straight line (i.e., dot dash line) with the same slope as that at the failure point was used to smoothly extend the axial strain-hoop strain curves, as indicated in Figs. 14-16. As seen from Figs. 14-16, the curves of UHPC-filled small FRP tube and hybrid bar specimens exhibited a first parabolic portion, second linear portion and a transition zone between them. The transition zone corresponds to the second stress reduction portion of the stress-strain curve of the specimen. The curvature of the transition zone is obviously dependent on the fibre winding angle, the FRP tube thickness and other variables, which will be discussed in detail in the next section.

3.5. Effect of various parameters

3.5.1 Fibre winding angle

The fibre winding angle had little effect on the initial stiffness of hybrid bar and UHPC-filled small FRP tube specimens, as shown in Fig. 10. However, the amount of stress reduction in the second or fourth portion of stress-strain curves of hybrid bars decreased with an increase in the fibre winding angle of the outer FRP tube. The amount of stress reduction in the second portion of stress-strain curves of UHPC-filled small FRP tube specimens also followed the similar trend. In addition, the slopes of the third strain hardening portion in the stress-strain curves of hybrid bar and UHPC-filled small FRP tube specimens as well as those of the fifth residual stress portion in the stress-strain curves of hybrid bar specimens increased with an increase in the fibre winding angle of the outer FRP tube. This is because FRP tubes with a larger fibre winding angle have a larger confinement stiffness. It was found that, for specimens with a fibre winding angle of ±45°, the slope of the fifth portion of hybrid bar specimens and the slope of the third portion of UHPC-filled small FRP tube specimens were close to zero. The ultimate axial strain of those specimens with fibre winding angles of ±45° was also found to be the largest among the specimens with other values of fibre winding angles, demonstrating their excellent deformation capacity.

It can be seen from Fig. 14 that the fibre winding angle had a significant influence on the dilation behaviour of both hybrid bar and UHPC-filled small FRP tube specimens. A larger fibre winding angle can lead to a smaller dilation of UHPC at a given axial strain. It can also be found that the slopes of the first parabolic portion, the second linear portion and the transition zone between them increased with the increase of the fibre winding angle.

3.5.2 Diameter of the central FRP bar

As seen from Fig. 11, the presence of the central FRP bar had no effect on the initial stiffness of hybrid bars; because of the close elastic modulus of the UHPC and the central FRP bar, as well as the good bonding between them with the presence of the ribs or sand-coated layer on the central FRP bar. However, the presence of the central FRP bar significantly alleviated the stress reduction in the second portion of UHPC-filled small FRP tube specimens, and the specimens with a central FRP bar (i.e., hybrid bars) had a higher compressive strength and a post-yielding stiffness. As discussed earlier, upon the failure of the central FRP bar, the behaviour of the fifth portion of hybrid bars was mainly dominated by the confinement of the outer FRP tube. As a result, the slope in this portion of the hybrid bar is almost the same as that of the third strain hardening portion of the corresponding UHPC-filled small FRP tube specimen. It was also found that the ε_{cu} values of hybrid bar and UHPC-filled small FRP tube specimens were similar, which can indicate that the actual hoop rupture strain of the outer FRP tube ($\varepsilon_{h,rup}$) was independent of the presence of the central FRP bar and the diameter of the central FRP bar.

As shown in Table 5, the compressive elastic modulus of GFRP bars with a nominal diameter of 25 mm was smaller than that of GFRP bars with a nominal diameter of 16 mm. In order to eliminate the influence of different compressive elastic modulus of the central FRP bar; the axial loads of hybrid bar specimens (P_{HB}) were normalized by the summation of axial loads of the corresponding UHPC (P_{UHPC}) and the central FRP bar (P_B) (i.e., $P_{HB}/(P_{UHPC}+P_B)$), and the axial strains (ε_c) were normalized by the axial strain at peak axial stress of UHPC ($\varepsilon_{co,UHPC}$) (i.e., $\varepsilon_c/\varepsilon_{co,UHPC}$), as shown in Fig. 17. The value of P_{UHPC} was taken as the product of the compressive strength of plain UHPC cylinders and the cross-sectional area of UHPC layer (i.e., $P_{UHPC}=f'_{co,UHPC}A_{UHPC}$). Similarly, the value of P_B was taken as the product of the axial stress of the central FRP bar at an axial strain of $\varepsilon_{co,UHPC}$ and its corresponding cross-sectional area (i.e., $P_B=E_B\varepsilon_{co,UHPC}A_B$, where E_B is the compressive elastic modulus of GFRP bars). Results from Fig. 17 can show that hybrid bars with a 25-mm-diameter central FRP bar were superior to those with a 16-mm-diameter central FRP bar before the central FRP bar failed. It was also found that the compressive strength of some hybrid bars with a 25-mm-diameter central FRP bar was slightly smaller than that of hybrid bars with a 16-mm-diameter central FRP bar (e.g., S2-C2-90-25-1/2/3 and S2-C2-90-16-1/2/3), which was due to the much smaller ultimate compressive strain of GFRP bars with a nominal diameter of 25 mm (see Table 5).

It can be seen from Fig. 15 that the axial strain-hoop strain curves of hybrid bar and UHPC-filled small FRP tube specimens were close. However, the presence of the central FRP bar had a slight effect on the dilation behaviour of hybrid bars. In comparison with UHPC-filled small FRP tube specimens, hybrid bar specimens had a shorter transition portion in the axial strain-hoop strain curves, corresponding to smaller stress drop in the second portion of their stress-strain curves. It was also found that there was a little difference in the dilation behaviour of hybrid bars with different central FRP bars.

3.5.3 Thickness of FRP tube

The stiffness, compressive strength and ultimate axial strain of both hybrid bar and UHPC-filled small FRP tube specimens increased with the increase of the outer FRP tube thickness (i.e., the increase of ultimate confining pressure provided by FRP), as seen from Fig. 12. The increase in the outer FRP tube thickness provided a contribution to eliminate the stress reduction or fluctuation in the second portion. Results from Fig. 16 can also show that specimens with a thicker FRP tube had smaller hoop strains at a certain axial strain, indicating that the increase of the FRP tube thickness can effectively inhibit the concrete expansion, which is consistent with the findings of other studies [31].

3.6. Behaviour of the central FRP bar in hybrid bars

For a given axial strain, the difference in axial loads between the hybrid bar and the UHPC-filled FRP tube with the same cross-sectional area as the UHPC layer of hybrid bars, is expected to represent the contribution of the axial load of the central FRP bar in a hybrid bar. In this study, the axial stress of the central FRP bar in a hybrid bar at a given axial strain is obtained from the following equation:

$$\sigma_B = (P_{HB} - f_{c,FU} A_{UHPC})/A_B \quad (1)$$

where P_{HB} is the total load of the hybrid bar; $f_{c,FU}$ is the axial stress of the corresponding UHPC-filled FRP tube specimen at a given axial strain based on the tests in this study; A_{UHPC} is the cross-sectional area of the UHPC layer in the hybrid bar; A_B is the cross-sectional area of the central FRP bar in the hybrid bar. When calculating the axial stress of the central FRP bar in a hybrid bar at a given axial strain, the contribution of the FRP tube is not accounted for although the axial load contribution of GFRP tube with a fibre winding angle of ±45° may be significant. This is because the contribution of FRP tube is existed in estimating the axial stresses of FRP-confined UHPC based on compression tests of the latter, and the axial load contribution of the FRP-confined UHPC is subtracted from that of the hybrid bar when calculating the axial stresses of the central FRP bar in a hybrid bar.

Figure 18 shows the comparison between the axial stress-axial strain behaviour of the central FRP bar in hybrid bars and the test results of the bare FRP bar (i.e., test results shown in Fig. 5c). It can be seen from Fig. 18 that the axial stress-axial strain behaviour of the central FRP bar in hybrid bars was superior to that of the corresponding bare FRP bar. One exception is Specimen S2-C1-90-16, which has a relatively small confinement stiffness. The initial stiffness of the central FRP bar, which was very close to that of the corresponding bare FRP bar, was independent of the level of FRP confinement, the FRP tube thickness and the fibre winding angle. However, the behaviour of the central FRP bar became non-linear and was greatly affected by the confinement of the outer FRP tube after the outer FRP tube was activated by the expansion of UHPC. A larger FRP confinement can lead to an enhanced compressive strength and an enhanced ultimate axial strain of the central FRP bar. Overall, the compressive strength of the central FRP bar in hybrid bars tested in the current study were much larger than that of the corresponding FRP bar in isolation, implying that the confinement provided by the outer FRP tube has a favorable effect on the effective exploitation of the compressive strength of the FRP bar. Although the central FRP bar in hybrid bars generally failed earlier than the outer FRP tube owing to the inherent properties of the material itself, the enhanced strength and strain of the central FRP bar in hybrid bars were still substantially beneficial to the axial performance of hybrid bars. It is demonstrated that the compressive strength of FRP bars can be well exploited in such a form of hybrid bars. The subsequent studies conducted by the authors have demonstrated the superiority of RC columns reinforced hybrid bars than the corresponding RC columns reinforced with FRP bars [43].

4. Transverse Shear Test and Results

4.1 Specimens preparation and test set-up

A total of 29 specimens, including 12 hybrid bars and 12 UHPC-filled small FRP tubes and 5 bare GFRP bars, were prepared and tested under transverse shear loading. All the hybrid bar specimens and UHPC-filled small FRP tube specimens adopted the same materials as the first batch of specimens (see Section 3), and thus the labeling system of the specimens presented in Section 3.1 was also adopted in this section. In addition, "FRP bar" was used to refer to a bare FRP bar specimen and a following number was used to distinguish the duplicate specimens. The main parameters concerned in this section include the fibre winding angle of the outer FRP tube, and the presence of the central FRP bar. The transverse shear strength tests of all the specimens were carried out in accordance with the methodology described in ACI 440.3 R-12 [44]. Figure 19 shows a steel double shear test device, which consists of a holder, one upper blade, and two lower blades. The detailed dimensions, as given in Fig. 19, are slightly different from the suggested dimensions in ACI 440.3 R-12 [44] to cater for the large diameter of the hybrid bars. The thickness of two lower blades was 12 mm and the thickness of upper blade was 36 mm. During the test, the holder was fixed to the framework of the testing machine and the upper blade ran perpendicularly to the specimen axis to ensure that the bar was under two-plane shear loading. All test specimens had a total length of 300 mm and they were loaded at a displacement-control rate of 1.5 mm/min (see Fig. 19).

4.2 Transverse shear results

Figure 20 presents the failure modes of all specimens. The test specimens were cut into three pieces, indicating that shear planes failed at the same time [21,45]. It was also found that some GFRP bar specimens experienced fibre delamination (Fig. 20h), which is consistent with the findings of other study [45]. In order to clearly identify the formation of failure surfaces in a hybrid bar during the test, Fig. 21 illustrates the axial load-displacement curves of hybrid bars and the reference specimens (i.e., UHPC-filled small FRP tube and GFRP bar) under transverse shear loading. The results show that hybrid bars have a two-stage formation of failure surfaces, corresponding to two peak loads, respectively: i) the first one was mainly caused by the shear failure of the outer FRP tube and the corresponding first peak load decreased with an increase in the fibre winding angle of the outer FRP tube; and ii) the second one was induced by the shear failure of the central FRP bar. However, the two peak loads of the hybrid bar were much larger than those of the reference specimens due to the optimal combination of each component and good interaction between them, which can demonstrate an excellent shear resistance of the hybrid bar. To further interpret the interaction between each component in a hybrid bar, Fig. 21 illustrates the summation of the loads of the corresponding UHPC-filled small FRP tube and the bare GFRP bar at a given displacement (represented by a purple line marked by circles). It is clearly shown that the shear resistance of the hybrid bar was significantly larger than the summation of shear resistance of UHPC-filled small FRP tube and that of the bare GFRP bar due to the small deformation capacity of UHPC-filled small FRP tube under transverse shear loading. The summation of these loads was slightly larger that of the hybrid bar at the initial stage. This was because the former included an additional load of UHPC with the same cross-sectional area as the central FRP bar. Although the contribution of the UHPC-filled small FRP tube part in the total shear load capacity was substantial, the deformation capacity of the UHPC-filled small FRP tube in isolation under shear was much smaller than that of the FPR bar (the ultimate deformation of the central FRP bar corresponded to the deformation at the second peak). It can be seen from Fig. 21 that the load decrease upon the first peak of the hybrid bar was caused by the failure of the UHPC-filled FRP tube section, while the load reduction of this stage was much smaller than the shear load capacity of the UHPC-filled FRP tube in isolation (see Fig. 21). Thus, it can be demonstrated that the UHPC-filled FRP tube and the central FRP bar in hybrid bars are in an optimum combination: the presence of the central FRP bar caused a delay in the failure of the UHPC-filled FRP tube section; and the shear loading after the first peak was jointly resisted by both the central FRP bar and the aggregate interlock action in UHPC, leading to an excellent shear load capacity (corresponding to the second peak) of hybrid bars.

The transverse shear strength (τ_u) can be obtained as follows:

$$\tau_u = \frac{P_s}{2A} \tag{2}$$

where P_s is the maximum failure force and A is the cross-sectional area of the specimen. Table 7 gives the transverse shear strength of all specimens. The thickness of the FRP tube was considered in the calculation of the cross-sectional areas of hybrid bars and UHPC-filled small FRP tube specimens. As hybrid bar have two different peak loads, both first and second transverse shear strengths were indicated in the present study. It can be seen from Table 7 that the fibre winding angle has a small effect on the second transverse shear strength of hybrid bars. However, the first transverse shear strength of both hybrid bar and UHPC-filled small FRP tube specimens decreased with an increase in the fibre winding angle of the outer FRP tube. In summary, the transverse shear resistance (e.g., shear load and deformation capacities) of hybrid bars is superior to that of the bare FRP bars.

5. Conclusions

This paper has presented experimental studies on the compressive and transverse shear behaviour of FRP-UHPC hybrid bars. The key parameters examined in the present study include the fibre winding angle of the FRP tube, fibre types of the FRP tube, the FRP tube thickness and the diameter of the central FRP bar. Based on the test results and discussions presented in this paper, the following conclusions can be drawn:

(1) Hybrid bars exhibit a five-portion average stress-strain response (i.e., an initial elastic portion, second stress fluctuation portion, third strain hardening portion, fourth stress reduction portion, and fifth residual stress portion). The third strain hardening portion is dependent on the confining stiffness; the stress-strain response of hybrid bars can be

designed to meet an elastic-plastic response like that of steel or a strong post-yielding strain-hardening response by using external FRP tubes with different stiffness.

(2) With an increase in the fibre winding angle of the outer FRP tube; the amount of the stress reduction in the second or fourth portion of stress-strain curves of hybrid bars and the amount of stress reduction in the second portion of stress-strain curves of UHPC-filled small FRP tube specimens decrease, and the slopes of both the third strain hardening portion and the fifth residual stress portion in the stress-strain curves of hybrid bars increase.

(3) The presence of the central FRP bar leads to little difference between the initial stiffnesses of the hybrid bar and the UHPC-filled small FRP tube due to the close elastic modulus of the two components (the UHPC and the FRP bar), while the presence of the central FRP bar leads to a smaller stress drop in the second portion of their stress-strain curves of hybrid bars. Hybrid bars with a 25-mm-diameter central FRP bar are superior to those with a 16-mm-diameter central FRP bar before the failure of the central FRP bar.

(4) The compressive strength and the ultimate axial strain of both hybrid bar and UHPC-filled small FRP tube specimens increase with the increase of the confinement stiffness from the outer FRP tube.

(5) The initial elastic modulus of the central FRP bar is independent of the level of FRP confinement, the FRP tube thickness and the fibre winding angle. The behavior of the central FRP bar is much superior to the bare FRP bar, because the ultimate axial strain (as well as the compressive strength) of the central FRP bar is substantially enhanced; which demonstrates that the confinement of the outer FRP tube are favorable in enhancing the compressive performance of the FRP bar in hybrid bars.

(6) Hybrid bars have a two-stage formation of failure surfaces under transverse shear loading, corresponding to two peaks of the shear load-deformation curves, respectively. The contribution of the UHPC-filled small FRP tube in the shear load capacity of hybrid bars is substantial, while the deformation capacity of the UHPC-filled small FRP tube in isolation under shear is much smaller than that of the FPR bar (the ultimate deformation of the central FRP bar corresponds to the deformation at the second peak). The

UHPC-filled small FRP tube and the central FRP bar in a hybrid bar are in an optimum combination, leading to an excellent shear load capacity.

To further examine the rationality and reliability of hybrid bars, tests on hybrid bar-reinforced concrete columns under different loadings (e.g. cyclic axial compression, eccentric compression and seismic loading) need to be carried out. Moreover, a design-oriented model proposed for hybrid bars should be established in the near future to enable the design of hybrid bars in various structural members.

Acknowledgements

The authors acknowledge the financial support received from the Natural Science Foundation of China (No. 52008116), the Guangzhou Science and Technology Department (No. 201904010163), the Natural Science Foundation of Guangdong Province (Nos. 2019A1515011637 and 2021B1515020029), the University of Macau (File no. UMMTP2020-MYSP-003), as well as the Association for Promotion of Science and Technology of Macau and the Office of China National Postdoctoral Council (File no. AM2020002).

References

[1] Zadeh, H. J. and Nanni, A. “Design of RC columns using glass FRP reinforcement.” J. Compos. Constr., 17 (3) (2012) 294-304,

[2] De Luca, A., Matta, F. and Nanni, A. “Behavior of full-scale glass fiber-reinforced polymer reinforced concrete columns under axial load.” ACI Struct. J., 107 (5) (2010) 589-596.

[3] Tobbi, H., Farghaly, A. S. and Benmokrane, B. “Concrete columns reinforced longitudinally and transversally with glass fiber-reinforced polymer bars.” ACI Struct. J., 109 (4) (2012) 551-558.

[4] Ali, M. A. and EI-Salakawy, E. “Seismic performance of GFRP-reinforced concrete rectangular columns.” J. Compos. Constr., 20 (3) (2016) 04015074.

[5] Pantelides, C. P., Gibbons, M. E. and Reaveley, L. “Axial load behavior of concrete columns confined with GFRP spirals”, J. Compos. Constr., 17(3) (2013) 305-313.

[6] Benmokrane, B., Mohamed, H. M. and Robert, M. "Case studies design, construction, and performance of continuously reinforced concrete pavement reinforced with GFRP bars: case study", J. Compos. Constr., ASCE 21 (4) (2017) 04017040.

[7] Hadi, M. N. S., Karim, H. and Sheikh, M. N. "Experimental investigations on circular concrete columns reinforced with GFRP Bars and helices under different loading conditions." J. Compos. Constr., 20 (4) (2016) 04016009.

[8] Teng, J.G., Zhang S. S. and Chen, J. F. "Strength model for end cover separation failure in RC beams strengthened with near-surface mounted (NSM) FRP strips", Engineering Structures, 110 (2016) 222-232.

[9] Khan, Q. S., Sheikh, M. N. and Hadi, M. N. 2015. "Tension and compression testing of fibre reinforced polymer (FRP) bars." *The 12th International Symposium on Fiber Reinforced Polymers for Reinforced Concrete Structures (FRPRCS-12) & The 5th Asia-Pacific Conference on Fiber Reinforced Polymers in Structures (APFIS-2015) Joint Conference* , Nanjing, China.

[10] Khorramian, K. and Sadeghian, P. New testing method of GFRP bars in compression, *CSCE Annual Conference 2018*, Fredericton, NB, Canada, Canadian Society for Civil Engineering, 2018.

[11] AlAjarmeh, O. S., Manalo, A. C., Benmokrane, B., Vijay, P. V., Ferdous, W. and Mendis, P. "Novel testing and characterization of GFRP bars in compression." Constr. Build. Mater., 225 (2019) 1112-1126.

[12] ACI 440.1R-15 (2015). Guide for The Design and Construction of Concrete Reinforced with FRP Bars. Farmington Hills, MI: ACI.

[13] CSA S806-12 (R2017). Design and Construction of Building Components with Fiber-Reinforced Polymers. Rexdale, ON, Canada.

[14] Nanni, A., Henneke, M. J. and Okamoto, T. "Tensile properties of hybrid rods for concrete reinforcement." Constr. Build. Mater., 8(1) (1994) 27-34.

[15] Wu, G., Wu, Z. S., Luo, Y. B., Sun, Z. Y. and Hu, X. Q. "Mechanical properties of steel-FRP composite bar under uniaxial and cyclic tensile loads." J. Mater. Civ. Eng., 22(10) (2010) 1056-1066.

[16] Wu, G., Sun, Z. Y., Wu, Z. S. and Luo, Y. B. "Mechanical properties of steel-FRP composite bars (SFCBs) and performance of SFCB reinforced concrete structures." Adv. Struct. Eng., 15(4) (2012) 625-635.

[17] Seo D. W., Park K. T., You Y. J. and Lee S. Y. "Experimental investigation for tensile performance of GFRP-steel hybridized rebar." Adv. Mater. Sci. Eng. 1 (2016) 1-12.

[18] Zhao, D., Pan, J., Zhou, Y., Sui, L. and Ye, Z. "New types of steel-FRP composite bar with round steel bar inner core: Mechanical properties and bonding performances in concrete." Constr. Build. Mater. 242 (2020) 118062.
[19] Liang, Y., Sun, C. and Ansari, F. "Acoustic emission characterization of damage in hybrid fiber-reinforced polymer rods." J. Compos. Constr. 8(1) (2004)70-18.
[20] You, Y. J., Park, Y. H., Kim, H. Y. and Park, J. S. "Hybrid effect on tensile properties of FRP rods with various material compositions." Compos. Struct., 80 (1) (2007) 117-122.
[21] Protchenko, K., Zayoud, F., Urbański, M. and Szmigiera, E. "Tensile and shear testing of basalt fiber reinforced polymer (BFRP) and hybrid basalt/carbon fiber reinforced polymer (HFRP) bars." Mater., 13 (24) (2020) 5839.
[22] Teng, J. G., Zhang, B., Zhang, S. S. and Fu, B. "Steel-free hybrid reinforcing bars for concrete structures", Adv. Struct. Eng., 21(11) (2018) 2617-2622.
[23] Shi, C., Wu, Z., Xiao, J., Wang, D., Huang, Z. and Fang Z. "A review on ultra high performance concrete: part I. Raw materials and mixture design", Constr. Build. Mater., 101 (2015) 741-751.
[24] Wille, K., El-Tawil, S. and Naaman, A. E. "Properties of strain hardening ultra high performance fiber reinforced concrete (UHP-FRC) under direct tensile loading." Cem. and Concr. Compos., 48 (2014) 53-66.
[25] Wille, K., Naaman, A. E. and Parra-Montesinos, G. J. "Ultra-high-performance concrete with compressive strength exceeding 150 MPa (22 ksi): a simpler way." ACI Mater. J., 108 (1) (2011) 46-54.
[26] Wille, K. and Boisvert-Cotulio, C. "Material efficiency in the design of ultra-high-performance concrete." Constr. Build. Mater., 86 (2015) 33-43.
[27] Li, J. Q., Wu, Z. M., Shi, C. J., Yuan, Q. and Zhang, Z. H. "Durability of ultra-high performance concrete – A review." Constr. Build. Mater., 255 (2020) 119296.
[28] Teng, J. G., Xiang, Y., Yu, T. and Fang, Z. "Development and mechanical behaviour of ultra-high-performance seawater sea-sand concrete." Adv. Struct. Eng., 22 (14) (2019) 3100-3120.
[29] Tian, H. Zhou, Z., Wei, Y., Wang, Y., Lu, J. "Experimental investigation on axial compressive behavior of ultra-high performance concrete (UHPC) filled glass FRP tubes", Constr. Build. Mater., 225 (2019) 678-691.
[30] Zohrevand, P., Mirmiran, A. "Behavior of ultrahigh-performance concrete confined by fiber-reinforced polymers", J. Mater. Civ. Eng., 23 (12) (2011) 1727-1734.

[31] Wang, W., Wu, C., Liu, Z. “Compressive behavior of ultra-high performance fiber-reinforced concrete (UHPFRC) confined with FRP”, Compos. Struct., 204 (2018) 419-437.
[32] Zeng, J. J., Ye, Y. Y., Gao, W. Y., Smith, S. T. and Guo, Y. C. “Stress-strain behavior of polyethylene terephthalate fiber-reinforced polymer-confined normal-, high- and ultra high-strength concrete.” J. Build. Eng., 30 (2020) 101243.
[33] GB 50010-2019. Code for Design of Concrete Structures. Beijing, China. (in Chinese)
[34] ACI 318-19 (2019). Building Code Requirements for Structural Concrete and Commentary. Farmington Hills, MI: ACI.
[35] ASTM C1856/C1856M (2017). Standard Practice for Fabricating and Testing Specimens of Ultra-High Performance Concrete, West Conshohocken, PA, USA.
[36] ASTM C469/C469M (2014). Standard Test Method for Static Modulus of Elasticity and Poisson Ratio of Concrete in Compression, West Conshohocken, PA: American Society for Testing and Materials (ASTM), USA.
[37] ASTM D3039-15 (2015). Standard Test Method for Tensile Properties of Polymer Matrix Composite Materials, West Conshohocken, PA: American Society for Testing and Materials (ASTM), USA.
[38] ASTM D2290-19 (2019). Standard Test Method for Apparent Hoop Tensile Strength of Plastic or Reinforced Plastic Pipe, West Conshohocken, PA: American Society for Testing and Materials (ASTM), USA.
[39] GB/T 5350 (2005). Fiber-Reinforced Thermosetting Plastics Composites-Determination for Longitudinal Compressive Properties. Beijing, China. (in Chinese)
[40] GB/T 30022-2013. Test Method for Basic Mechanical Properties of Fiber Reinforced Polymer Bar. Beijing, China. (in Chinese)
[41] Lam, L. and Teng, J.G. “Design-oriented stress-strain model for FRP-confned concrete.” Constr. Build. Mater., 17 (6-7) (2003) 471-489.
[42] Zeng, J. J., Duan, Z. J., Guo, Y. C. Xie, Z. H. and Li, L. J. “Novel fiber-reinforced polymer cross wrapping strengthening technique: a comparative study.” Adv. Struct. Eng., 23 (5) (2020) 979-996.
[43] Zeng, J. J., Ye, Y. Y., Yu, T. and Teng, J.G. “Axial compression tests on steel-free concrete columns reinforced longitudinally with hybrid bars.” in preparation.
[44] ACI 440.3R-12 (2012). Guide Test Methods for Fiber-Reinforced Polymers (FRPs) for Reinforcing or Strengthening Concrete Structures. Farmington Hills, MI: ACI.

[45] Genikomsou, A. S., Balomenos, G. P., Arczewska, P. and Polak, M. A. "Transverse shear testing of GFRP bars with reduced cross sections." J. Compos. Constr., 22 (5) (2018) 4018041.

TABLES AND FIGURES

TABLE CAPTIONS

Table 1. UHPC mix proportions (in weight)

Cement (P·II 52.5R)	Quartz powder	Silica fume	Sand	Water	Super-plasticizer
1.00	0.37	0.25	1.10	0.19	0.04

Table 2. Properties of UHPC

Batch	Compressive strength $f'_{co,UHPC}$ (MPa)	Ultimate axial strain $\varepsilon_{co,UHPC}$	Compressive elastic modulus $E_{c,UHPC}$ (GPa)	Poison's ratio μ
1	163.3	0.0033	50.3	0.20
2	142.3	0.0032	47.7	0.19

Table 3. Tensile properties of small GFRP tubes

Fibre winding angle （°）	Thickness (mm)	Number of FRP layers	Secant elastic modulus (GPa)
±45	2.90	4	3.71
±60	2.25	4	18.31
±80	1.81	4	38.72
±80	2.57	6	43.33

Table 4. Compressive properties of small GFRP tubes

Fibre winding angle （°）	Compressive strength (MPa)	Peak strain	Secant elastic modulus (GPa)	Poison's ratio
±45	93.69	0.0189	4.98	0.85
±60	98.86	0.0199	4.98	0.34
±80	86.35	0.0130	6.74	0.14

Table 5. Tensile and compressive properties of GFRP bars

Nominal diameter (mm)	Tensile elastic modulus (GPa)	Tensile strength (MPa)	Ultimate tensile strain	Compressive elastic modulus (GPa)	Compressive strength (MPa)	Ultimate compressive strain
25	41.0	711.6	0.0172	40.6	274.5	0.0077
16	47.6	892.2	0.0187	49.1	650.3	0.0121

Table 6. Details of specimens

Specimen	Batch	FRP type	Number of FRP layers	FRP thickness (mm)	Fibre winding angle（°）	Diameter of the central FRP bar (mm)
S1-G4-45-0-1/2/3	1	GFRP	4	2.90	45	N.A.
S1-G4-45-25-1/2/3	1	GFRP	4	2.90	45	25
S1-G4-60-0-1/2/3	1	GFRP	4	2.25	60	N.A.
S1-G4-60-25-1/2/3	1	GFRP	4	2.25	60	25
S1-G4-80-0-1/2/3	1	GFRP	4	1.81	80	N.A.
S1-G4-80-25-1/2/3	1	GFRP	4	1.81	80	25
S2-C1-90-0-1/2/3	2	CFRP	1	0.167	90	N.A.
S2-C1-90-25-1/2/3	2	CFRP	1	0.167	90	25
S2-C1-90-16-1/2/3	2	CFRP	1	0.167	90	16
S2-C2-90-0-1/2/3	2	CFRP	2	0.334	90	N.A.

S2-C2-90-25-1/2/3	2	CFRP	2	0.334	90	25
S2-C2-90-26-1/2/3	2	CFRP	2	0.334	90	16
S2-G4-80-0-1/2/3	2	GFRP	4	1.81	80	N.A.
S2-G4-80-25-1/2/3	2	GFRP	4	1.81	80	25
S2-G4-80-16-1/2/3	2	GFRP	4	1.81	80	16
S2-G6-80-0-1/2/3	2	GFRP	6	2.57	80	N.A.
S2-G6-80-25-1/2/3	2	GFRP	6	2.57	80	25

Note: N.A. —— Not applicable.

Table 7. Key results of specimens under transverse shear tests

Specimen		First transverse shear strength τ_{u1}	Mean	Standard deviation	Second transverse shear strength τ_{u2}	Mean	Standard deviation
Hybrid bar	S1-G4-45-25-1	70.1	68.3	2.32	66.7	64.5	3.09
	S1-G4-45-25-2	69.0			60.1		
	S1-G4-45-25-3	64.9			66.6		
	S1-G4-45-25-4	69.2			64.4		
	S1-G4-60-25-1	58.3	60.1	3.91	67.5	65.6	1.29
	S1-G4-60-25-2	56.1			65.0		
	S1-G4-60-25-3	60.9			64.6		
	S1-G4-60-25-4	65.2			65.4		
	S1-G4-80-25-1	51.2	50.1	1.58	67.6	66.3	1.38
	S1-G4-80-25-2	51.3			66.1		
	S1-G4-80-25-3	47.9			64.4		
	S1-G4-80-25-4	50.0			66.9		
UHPC-filled small FRP tube	S1-G4-45-0-1	42.6	44.1	2.60	N.A.	N.A.	N.A.
	S1-G4-45-0-2	41.6			N.A.		
	S1-G4-45-0-3	47.5			N.A.		
	S1-G4-45-0-4	44.6			N.A.		
	S1-G4-60-0-1	27.9	30.1	1.52	N.A.	N.A.	N.A.
	S1-G4-60-0-2	30.9			N.A.		
	S1-G4-60-0-3	30.8			N.A.		
	S1-G4-60-0-4	31.0			N.A.		
	S1-G4-80-0-1	17.3	19.1	2.69	N.A.	N.A.	N.A.
	S1-G4-80-0-2	22.7			N.A.		
	S1-G4-80-0-3	19.7			N.A.		
	S1-G4-80-0-4	16.8			N.A.		
GFRP bar	FRP bar-1	165.7	160.7	6.97	N.A.	N.A.	N.A.
	FRP bar-2	155.8			N.A.		
	FRP bar-3	161.9			N.A.		
	FRP bar-4	168.5			N.A.		
	FRP bar-5	151.6			N.A.		

FIGURE CAPTIONS

Fig. 1. FRP-UHPC hybrid bar

Fig. 2. FRP bar-reinforced concrete columns (FBRCCs) and hybrid bar-reinforced concrete columns (HBRCCs)

Fig. 3. Split disk tests on small GFRP tubes

Fig. 4. Compression tests on small GFRP tubes

Fig. 5. Tensile and compression tests on GFRP bars

Fig. 6. Preparation of hybrid bar specimens

Fig. 7. Levelling at two ends

Fig. 8. Compression test set-up

Fig. 9. Typical failure modes of specimens under axial compression tests

Fig. 10. Effect of fiber winding angles on the axial compressive behaviour of specimens

Fig. 11. Effect of the presence of the central FRP bar on the axial compressive behaviour of specimens

Fig. 12. Effect of the thickness of the outer FRP tube on the axial compressive behaviour of specimens

Fig. 13. Typical axial stress-axial strain diagrams of hybrid bar and UHPC-filled FRP tube specimens

Fig. 14. Effect of fiber winding angles on the dilation behaviour of specimens

Fig. 15. Effect of the diameter of the central FRP bar on the dilation behaviour of specimens

Fig. 16. Effect of the thickness of the outer FRP tube on the dilation behaviour of specimens

Fig. 17. Normalized axial stress-axial strain curves of hybrid bars with different central FRP bars

Fig. 18. Axial stress-axial strain behaviour of the central FRP bar in hybrid bars

Fig. 19. Transverse shear test set-up

Fig. 20. Typical failure modes of specimens under transverse shear tests

Fig. 21. Load-displacement curves of specimens under transverse shear tests

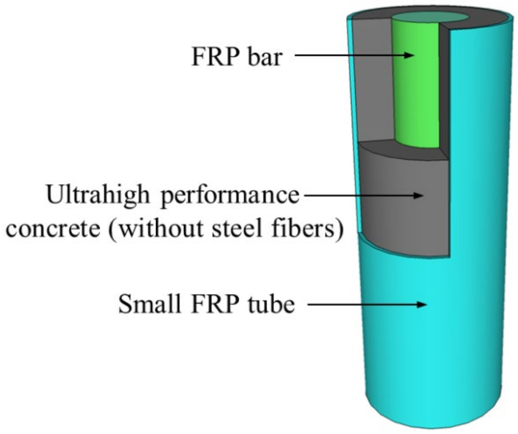

Fig. 1. FRP-UHPC hybrid bar

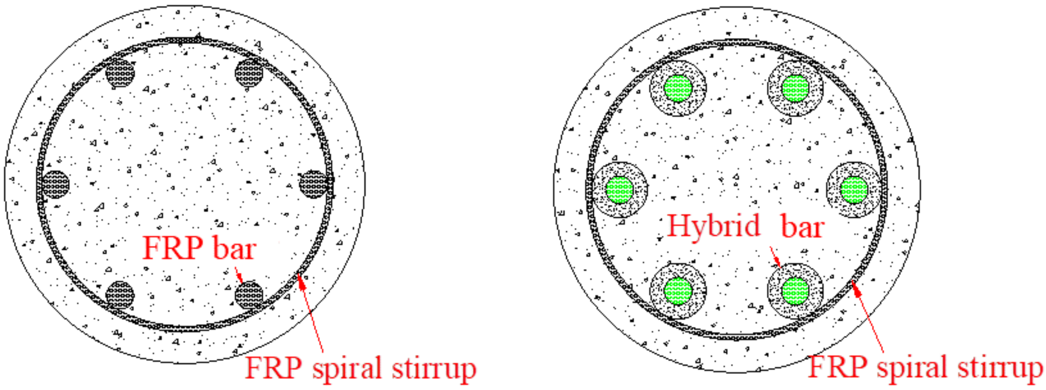

(a) Cross-section of FBRCCs (b) Cross-section of HBRCCs

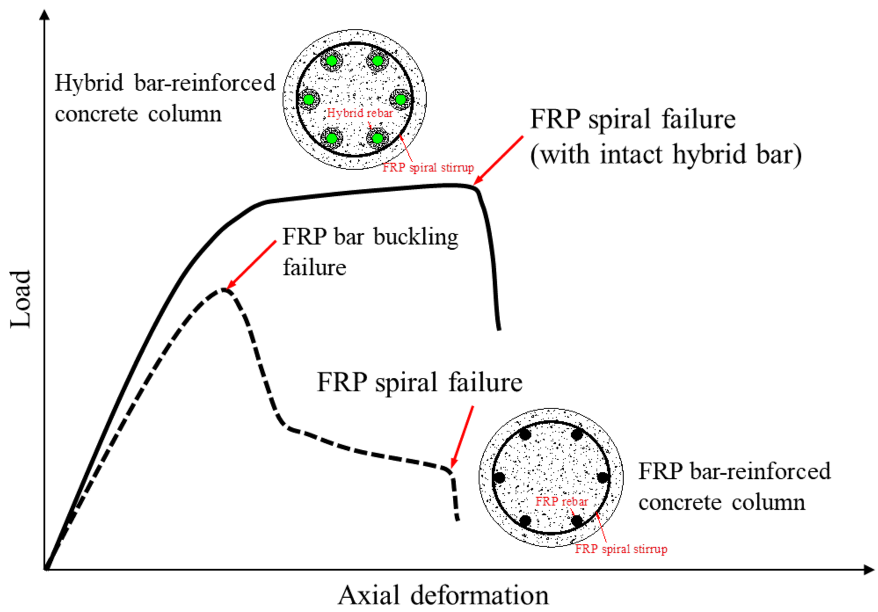

(c) Diagrammatic sketch of load-deformation responses of FBRCCs and HBRCCs

Fig. 2. FRP bar-reinforced concrete columns (FBRCCs) and hybrid bar-reinforced concrete columns (HBRCCs)

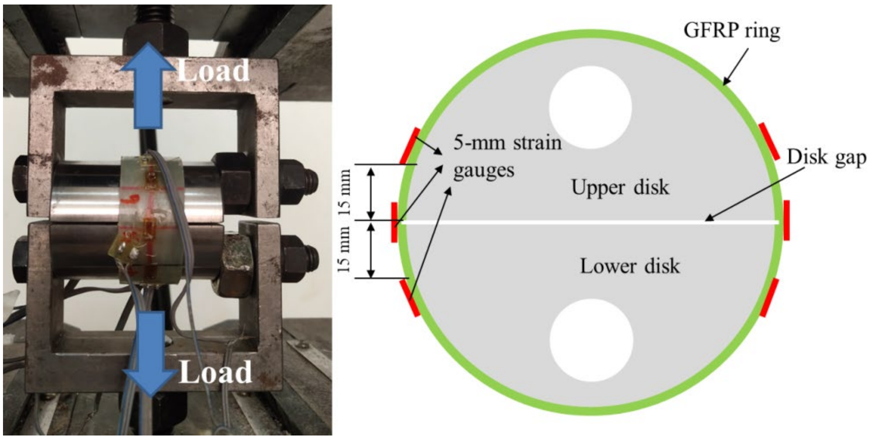

(a) Test set-up and layouts of strain gauges

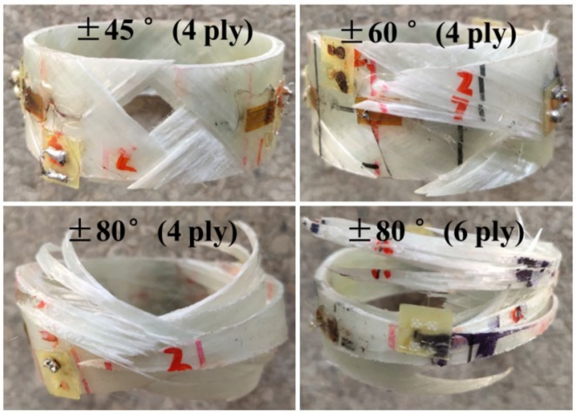

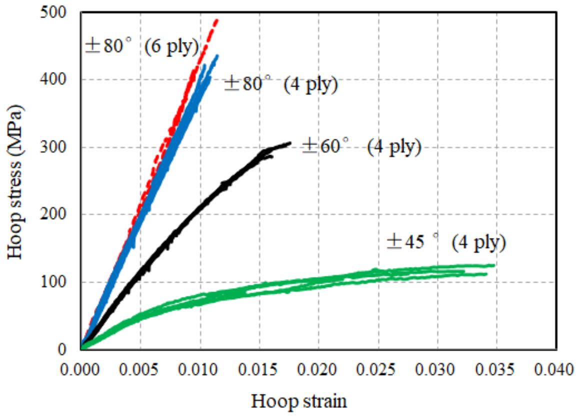

(b) Typical failure modes (c) Hoop stress-hoop strain curves

Fig. 3. Split disk tests on small GFRP tubes

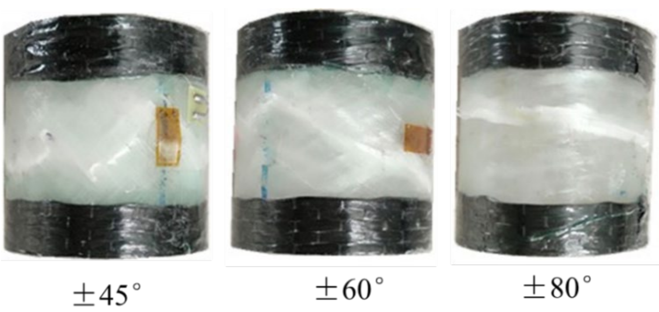

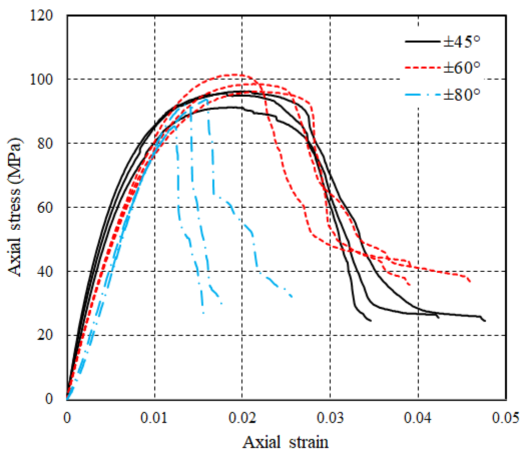

(a) Typical failure modes (b) Stress-strain curves

Fig. 4. Compression tests on small GFRP tubes

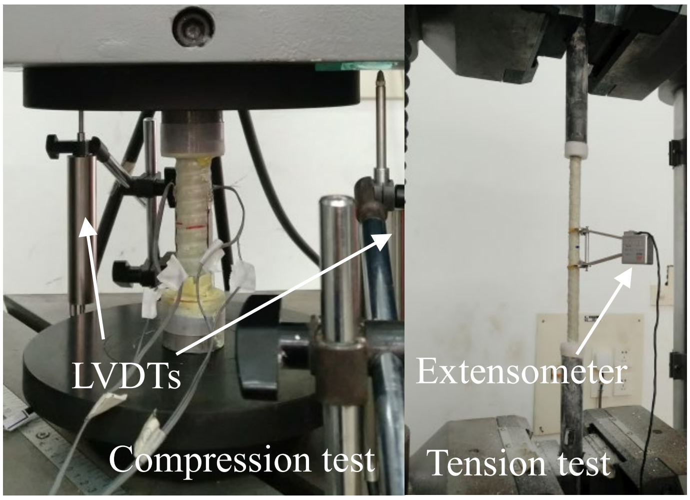

(a) Test set-up

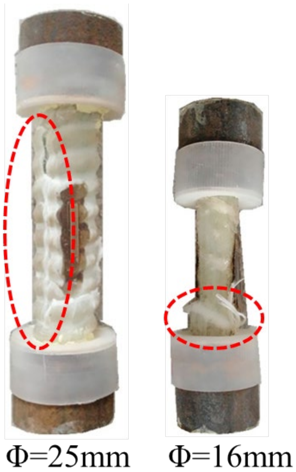

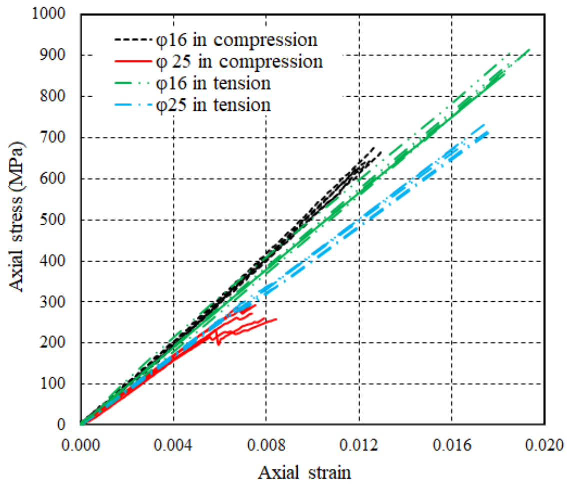

(b) Failure modes of GFRP bars in compression (c) Stress-strain curves

Fig. 5. Tensile and compression tests on GFRP bars

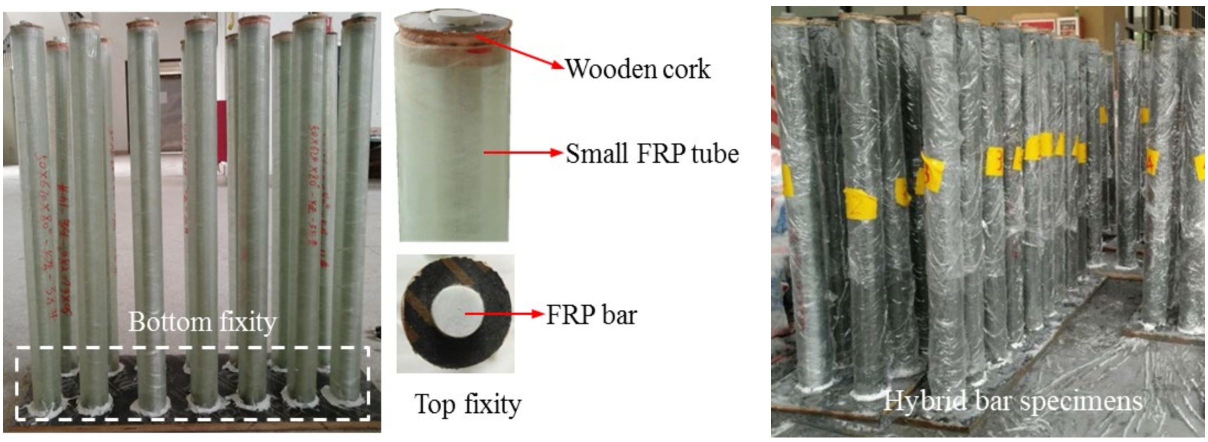

Fig. 6. Preparation of hybrid bar specimens

Fig. 7. Levelling at two ends

Fig. 8. Compression test set-up

(a) S1-G4-45-0-3 (b) S1-G4-45-25-1 (c) S1-G4-60-25-1 (d) S1-G4-80-25-3

(e) S2-G4-80-0-2 (f) S2-C1-90-25-2 (g) S2-C2-90-16-2 (h) S2-C2-90-0-1

(i) UHPC core (j) UHPC layer and central FRP bar

Fig. 9. Typical failure modes of specimens under axial compression tests

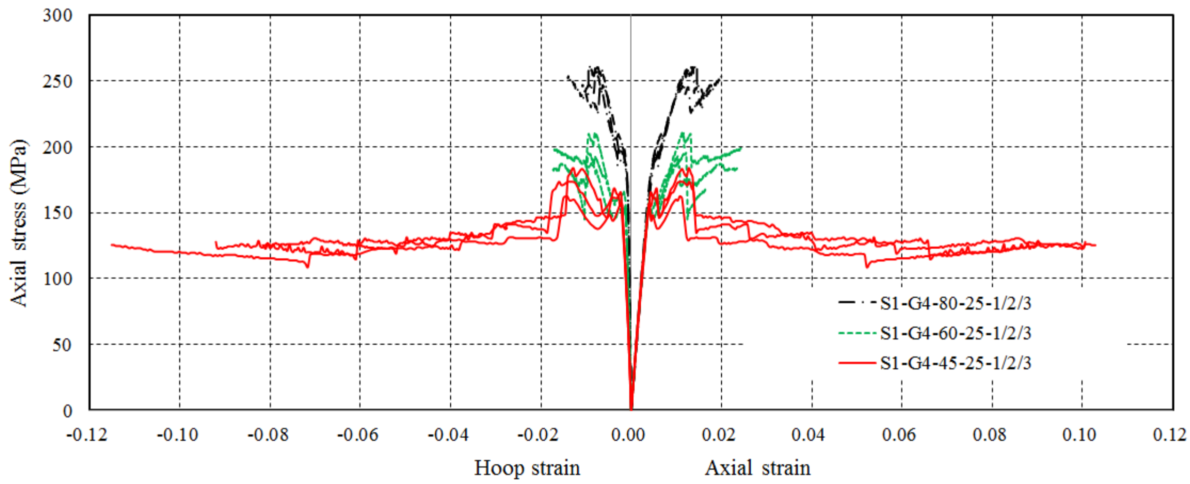

(a) Hybrid bar

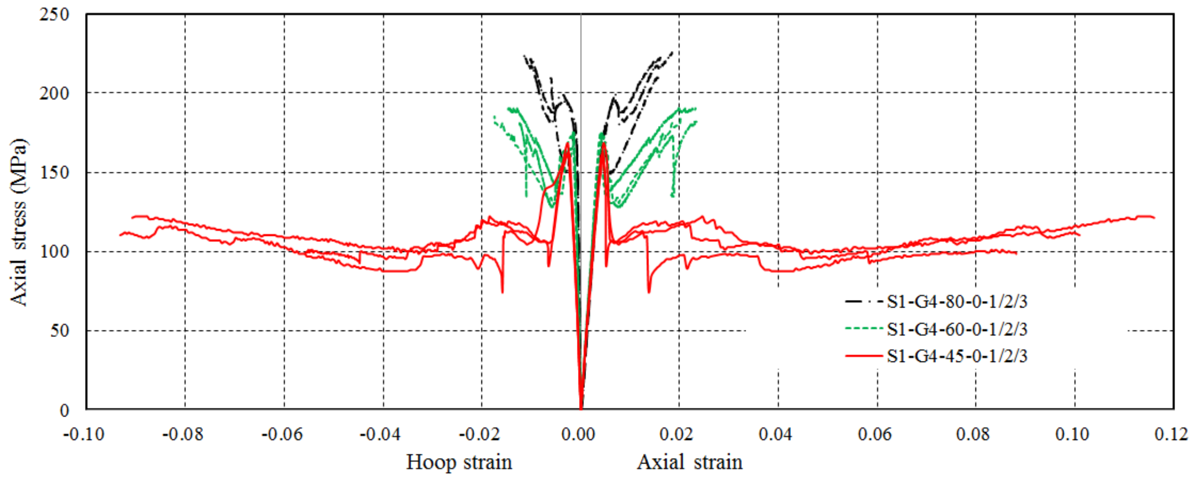

(b) UHPC-filled small FRP tube

Fig. 10. Effect of fiber winding angles on the axial compressive behaviour of specimens

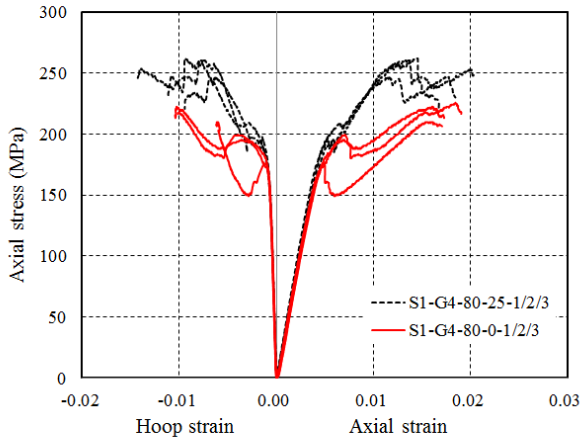

(a) GFRP = 4ply, 80°

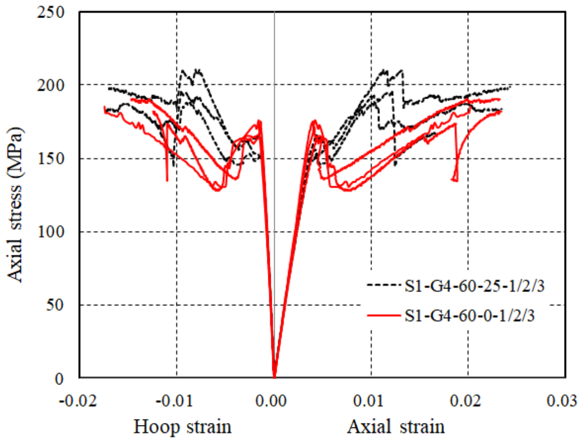

(b) GFRP = 4ply, 60°

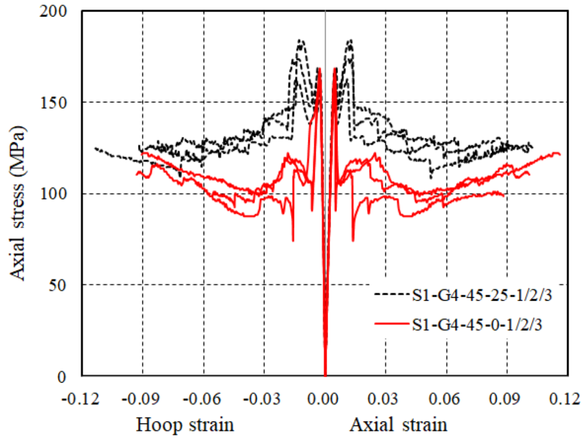

(c) GFRP = 4ply, 45°

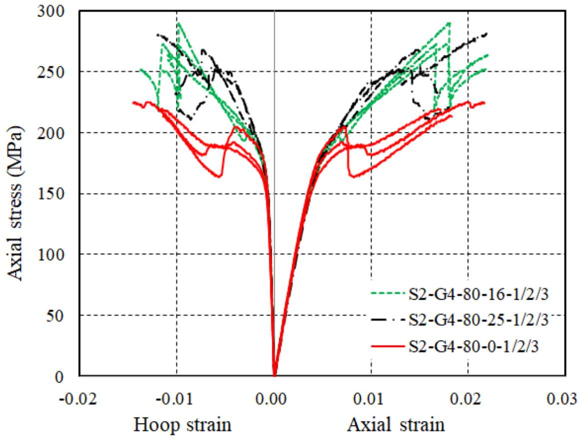

(d) GFRP = 4ply, 80° (S2)

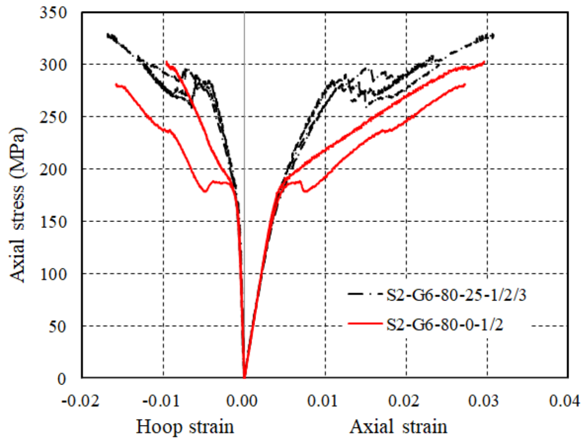

(e) GFRP = 6ply, 80°

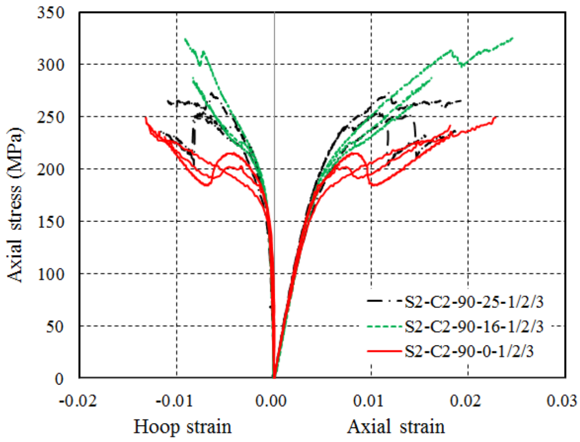

(f) CFRP = 2ply, 90°

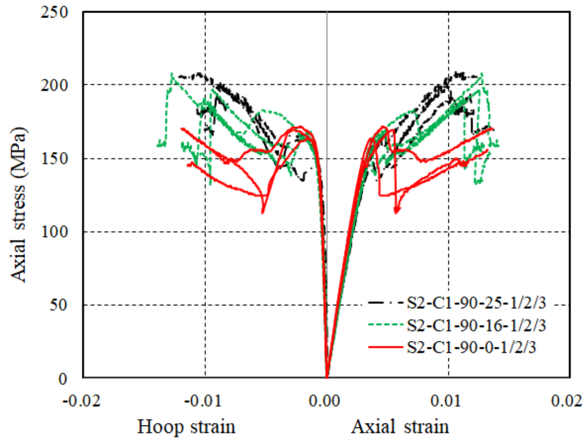

(g) CFRP = 1ply, 90°

Fig. 11. Effect of the presence of the central FRP bar on the axial compressive behaviour of specimens

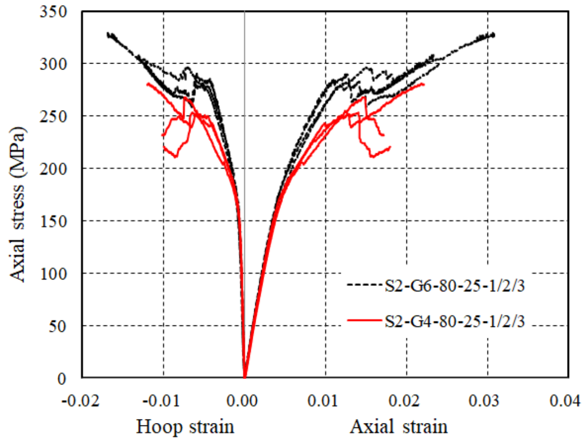

(a) GFRP (80°), 25-mm-diameter FRP bar

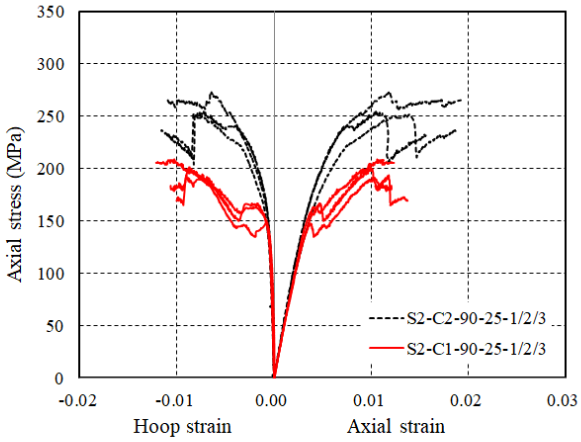

(b) CFRP (90°), 25-mm-diameter FRP bar

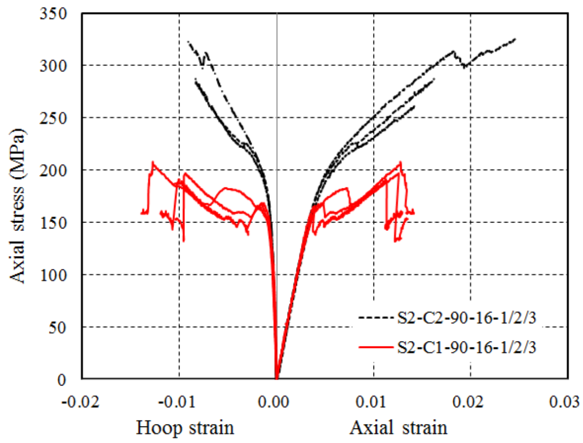

(c) CFRP (90°), 16-mm-diameter FRP bar

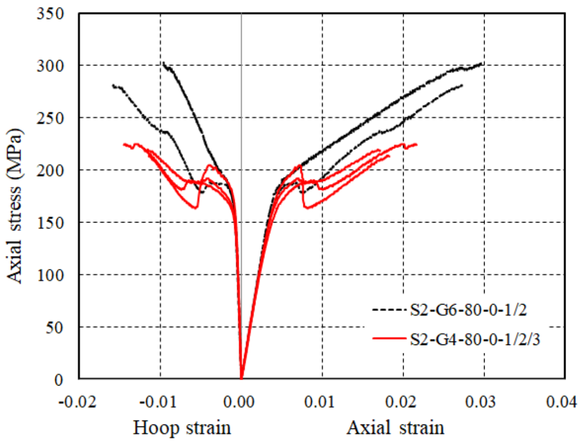

(d) GFRP (80°)

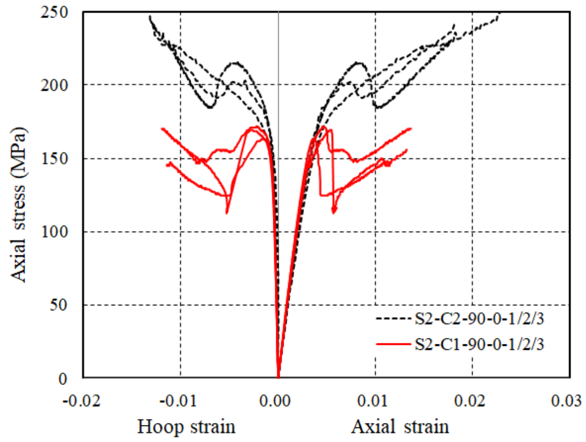

(e) CFRP (90°)

Fig. 12. Effect of the thickness of the outer FRP tube on the axial compressive behaviour of specimens

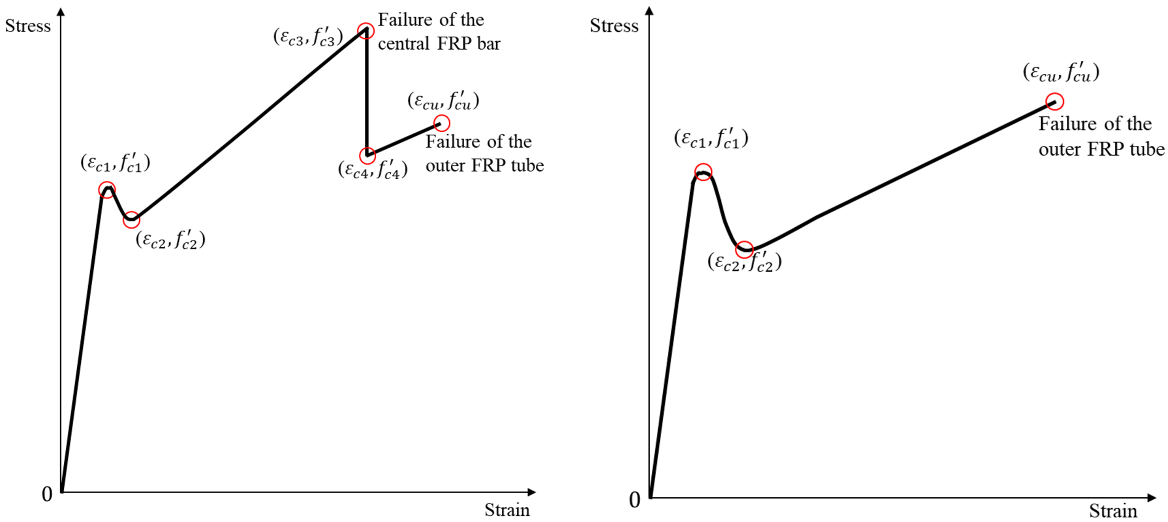

(a) Hybrid bar (b) UHPC-filled FRP tube

Fig. 13. Typical axial stress-axial strain diagrams of hybrid bar and UHPC-filled FRP tube specimens

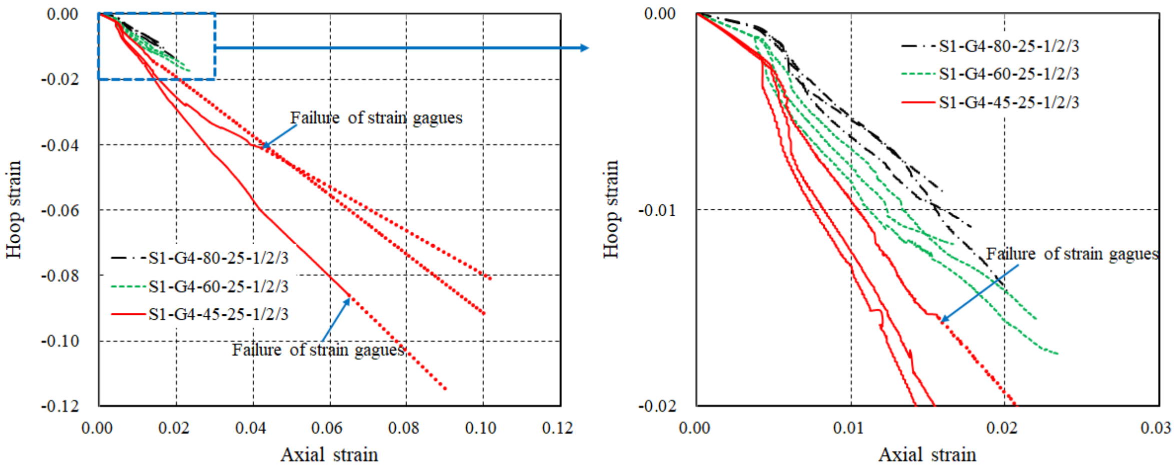

(a) Hybrid bar

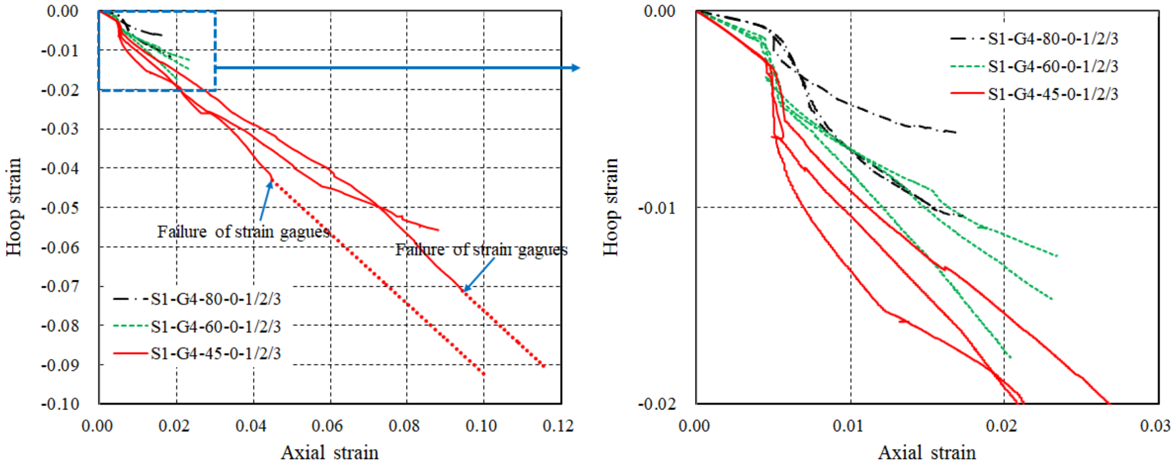

(b) UHPC-filled small FRP tube

Fig. 14. Effect of fiber winding angles on the dilation behaviour of specimens

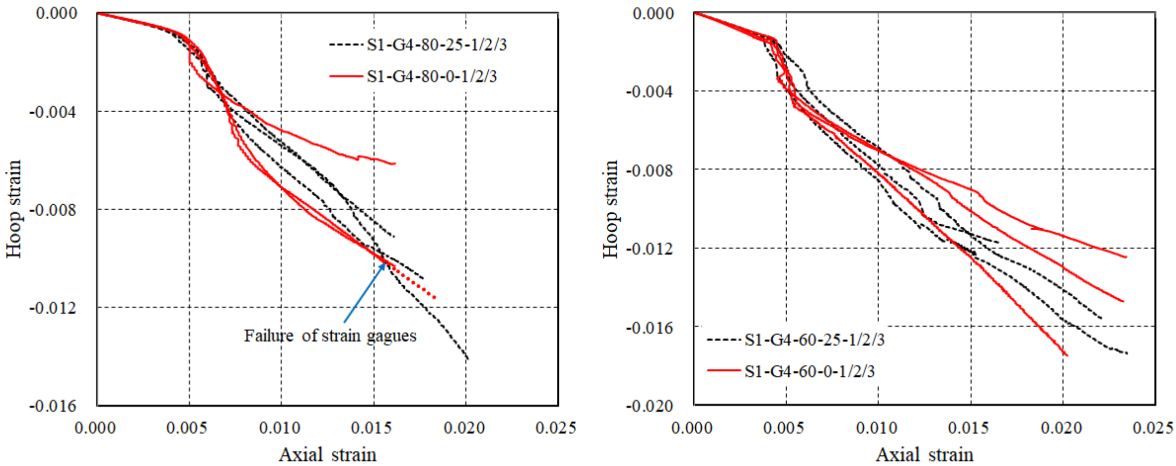

(a) GFRP = 4ply, 80°　　(b) GFRP = 4ply, 60°

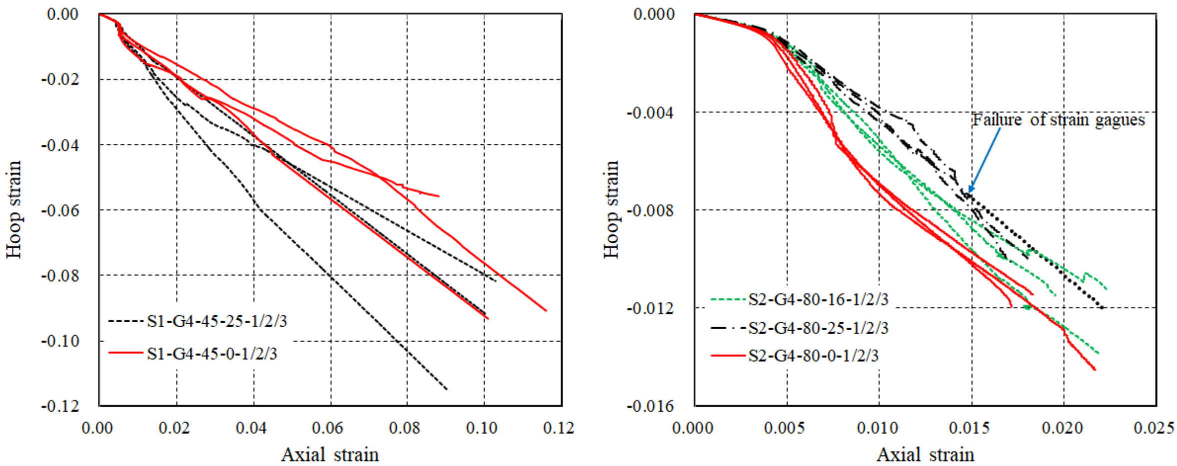

(c) GFRP = 4ply, 45°　　(d) GFRP = 4ply, 80° (S2)

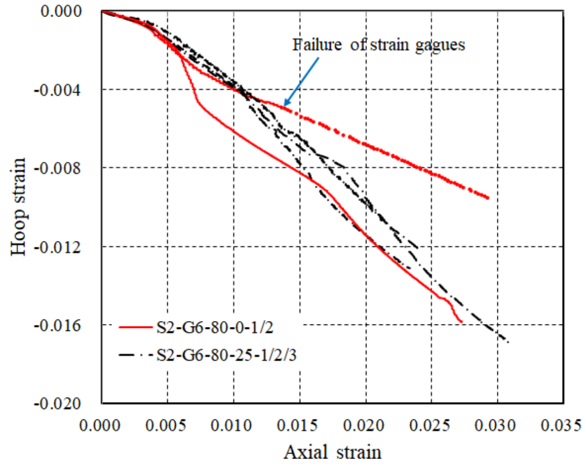

(e) GFRP = 6ply, 80°

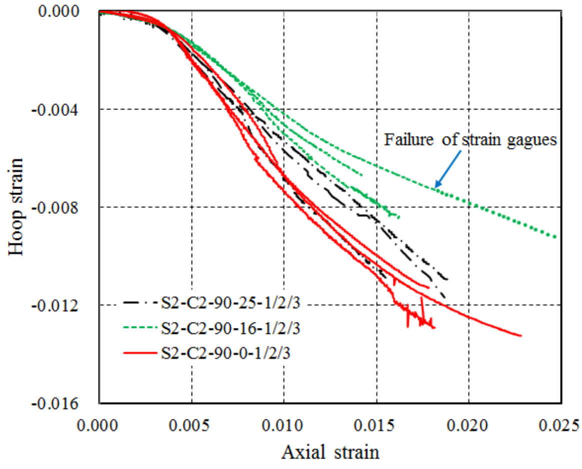

(f) CFRP = 2ply, 90°

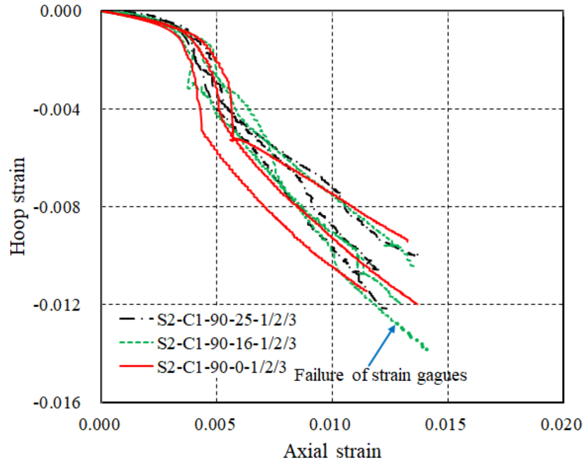

(g) CFRP = 1ply, 90°

Fig. 15. Effect of the diameter of the central FRP bar on the dilation behaviour of specimens

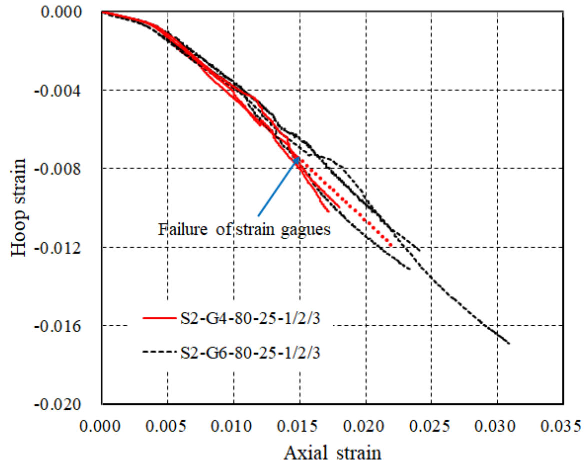

(a) GFRP (80°), 25-mm-diameter FRP bar

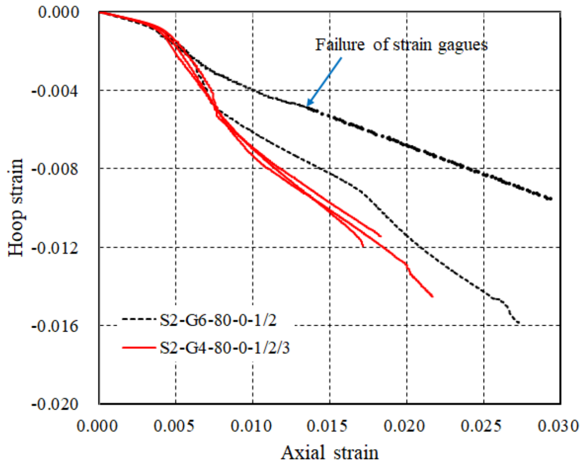

(b) GFRP (80°)

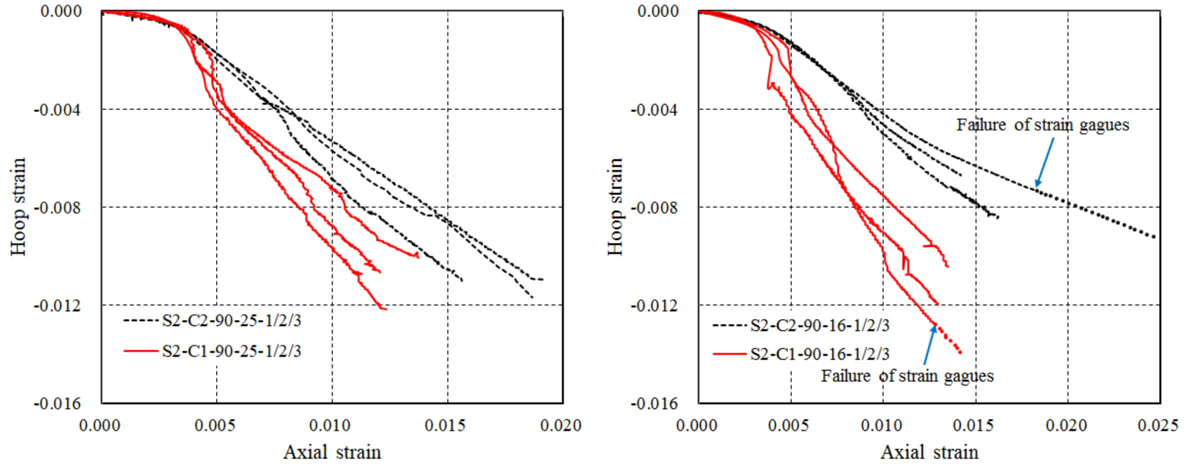

(c) CFRP (90°), 25-mm-diameter FRP bar　　(d) CFRP (90°), 16-mm-diameter FRP bar

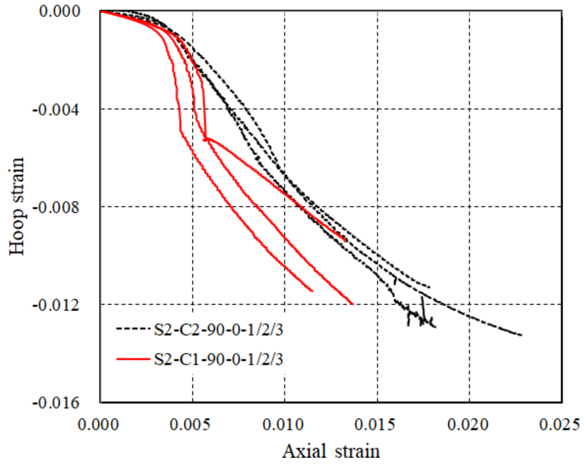

(e) CFRP (90°)

Fig. 16. Effect of the thickness of the outer FRP tube on the dilation behaviour of specimens

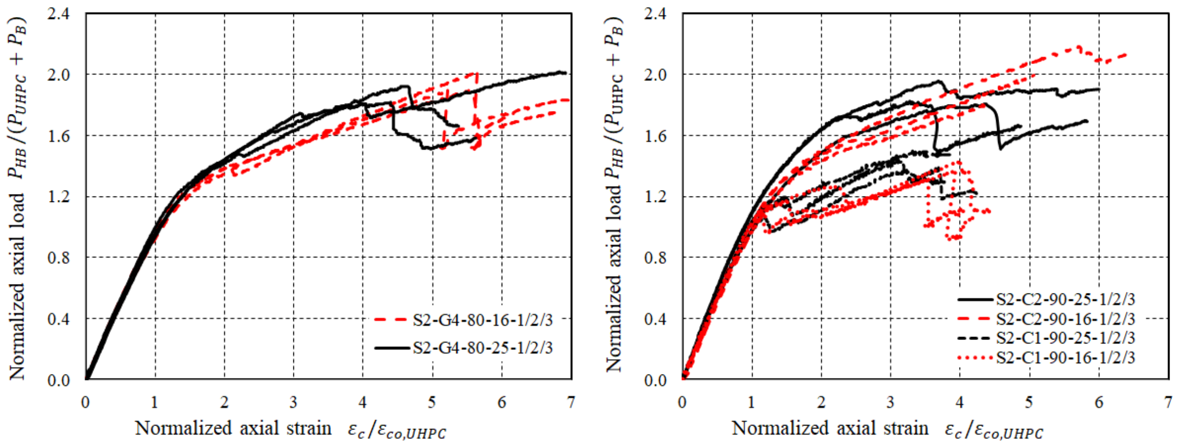

(a) GFRP = 4ply, 80° (S2)　　(b) CFRP, 90°

Fig. 17. Normalized axial stress-axial strain curves of hybrid bars with different central FRP bars

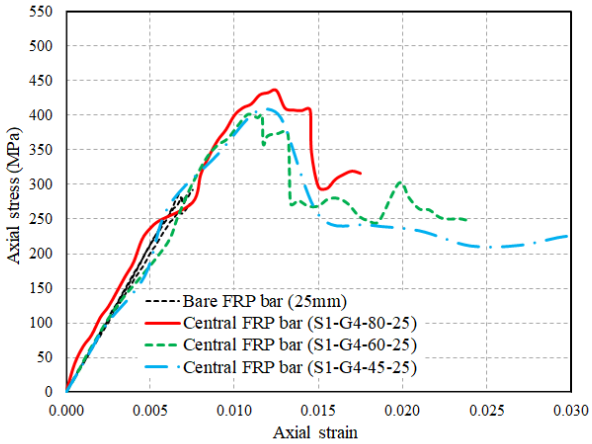

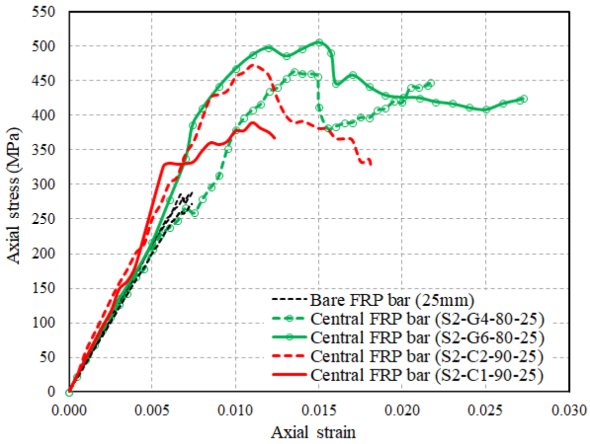

(a) Effect of fiber winding angle (25mm) (b) Effect of FRP tube thickness (25mm)

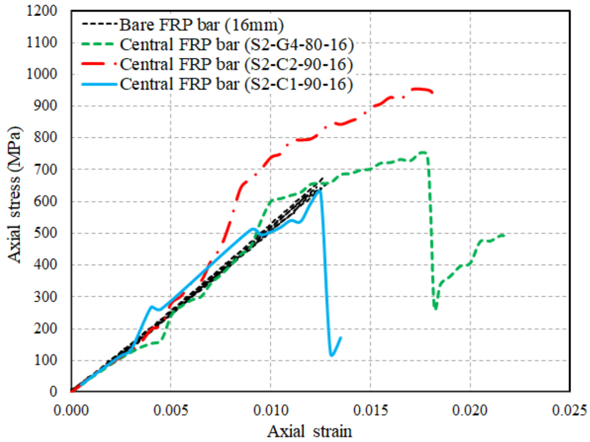

(c) Effect of FRP tube thickness (16mm)

Fig. 18. Axial stress-axial strain behaviour of the central FRP bar in hybrid bars

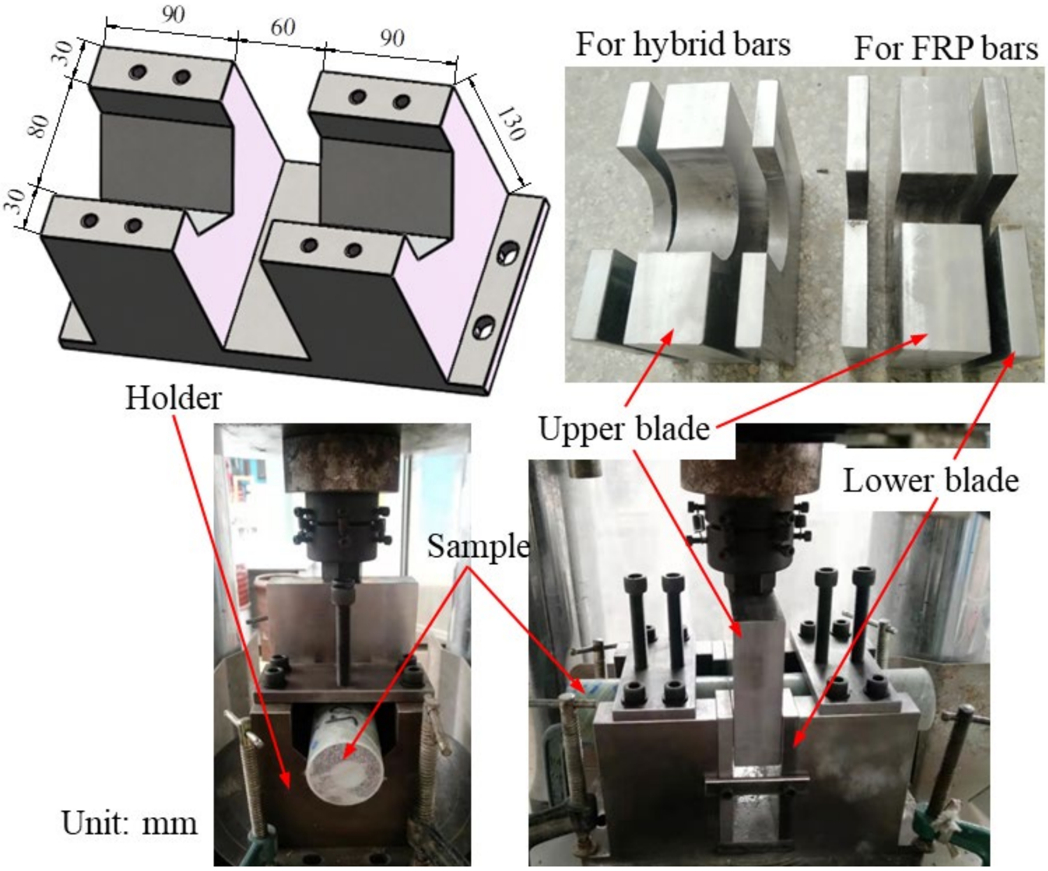

Fig. 19. Transverse shear test set-up

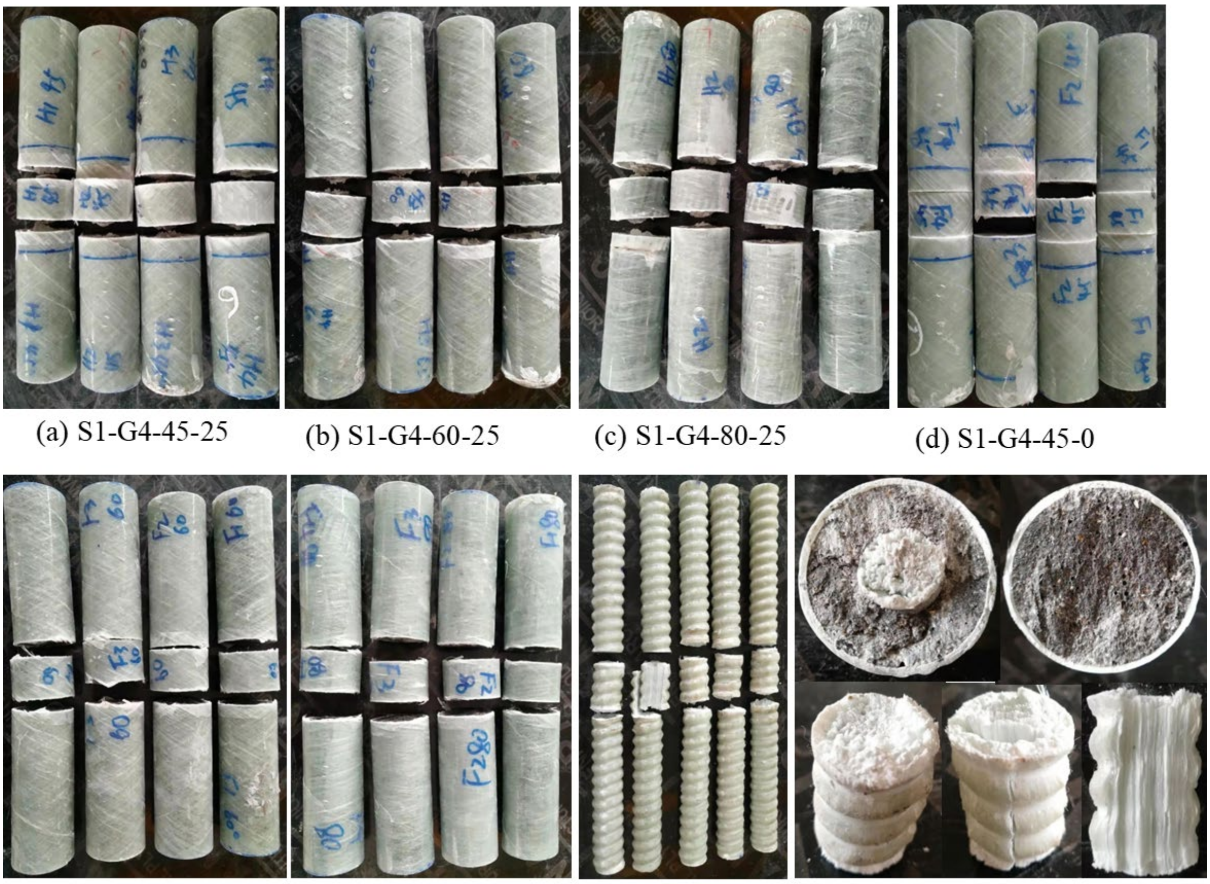

(a) S1-G4-45-25 (b) S1-G4-60-25 (c) S1-G4-80-25 (d) S1-G4-45-0

(e) S1-G4-60-0 (f) S1-G4-80-0 (g) FRP bar (h) Shear failure surfaces

Fig. 20. Typical failure modes of specimens under transverse shear tests

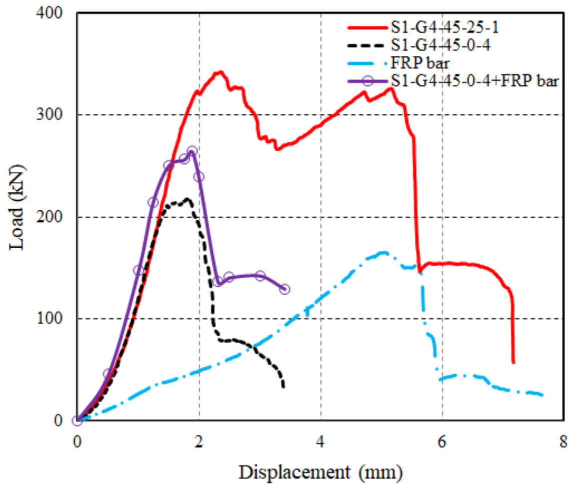

(a) Fibre winding angle = ±45°

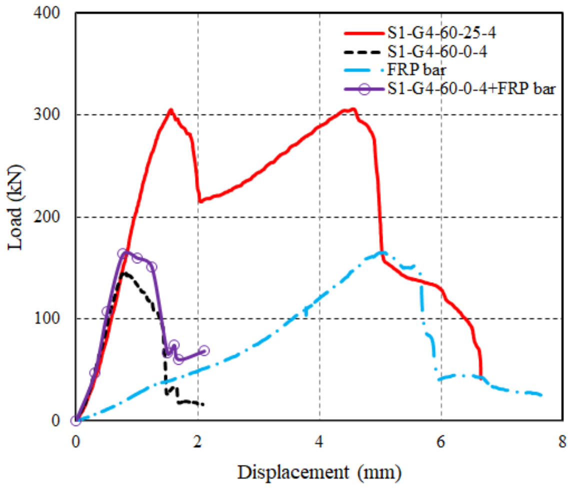

(b) Fibre winding angle = ±60°

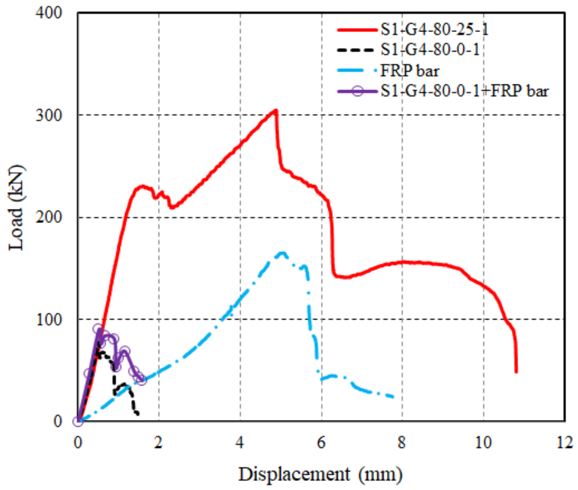

(c) Fibre winding angle = ±80°

Fig. 21. Load-displacement curves of specimens under transverse shear tests

APPENDIX

Table A1. Key results of specimens under axial compression tests

Specimen	f'_{c1}	f'_{c2}	f'_{c3}	f'_{c4}	f'_{cu}	ε_{c1}	ε_{c2}	ε_{c3}	ε_{c4}	ε_{cu}	$\varepsilon_{h,rup}$
S1-G4-80-25-1	209.73	205.52	261.95	236.69	246.79	0.0066	0.0068	0.0146	0.0156	0.0178	-0.0109
S1-G4-80-25-2	193.73	189.52	246.79	240.90	231.63	0.0056	0.0058	0.0117	0.0121	0.0161	-0.0091
S1-G4-80-25-3	196.26	185.31	260.27	240.90	252.69	0.0060	0.0059	0.0138	0.0140	0.0201	-0.0141
S1-G4-60-25-1	164.25	156.67	195.41	144.88	166.77	0.0048	0.0054	0.0122	0.0124	0.0166	-0.0117
S1-G4-60-25-2	153.30	145.72	187.83	169.30	183.62	0.0044	0.0050	0.0104	0.0109	0.0234	-0.0174
S1-G4-60-25-3	155.83	150.77	210.57	184.46	198.78	0.0043	0.0044	0.0116	0.0134	0.0243	-0.0171
S1-G4-45-25-1	160.88	136.45	162.56	128.87	125.50	0.0042	0.0057	0.0112	0.0120	0.0905	-0.1151 (-0.0860)
S1-G4-45-25-2	168.19	145.41	183.08	146.29	127.89	0.0057	0.0063	0.0125	0.0141	0.1006	-0.0920 (-0.0155)
S1-G4-45-25-3	172.57	148.92	175.20	131.40	125.27	0.0047	0.0066	0.0118	0.0141	0.1028	-0.0817 (-0.0410)
S2-C1-90-16-1	168.46	154.98	197.10	133.08	153.30	0.0048	0.0050	0.0126	0.0126	0.0135	-0.0104
S2-C1-90-16-2	181.09	166.77	208.05	158.35	158.35	0.0065	0.0078	0.0127	0.0135	0.0141	-0.0139 (-0.0128)
S2-C1-90-16-3	165.93	138.14	191.20	143.19	158.35	0.0039	0.0040	0.0112	0.0114	0.0129	-0.0120
S2-C1-90-25-1	166.77	149.93	201.31	179.41	183.62	0.0047	0.0051	0.0099	0.0107	0.0121	-0.0106
S2-C1-90-25-2	163.41	157.51	208.89	203.84	205.52	0.0041	0.0047	0.0106	0.0113	0.0123	-0.0121
S2-C1-90-25-3	147.40	134.77	193.73	165.93	169.30	0.0038	0.0041	0.0118	0.0121	0.0137	-0.0100
S2-C2-90-16-1	N.A.	N.A.	N.A.	N.A.	261.11	N.A.	N.A.	N.A.	N.A.	0.0142	-0.0067
S2-C2-90-16-2	N.A.	N.A.	N.A.	N.A.	287.22	N.A.	N.A.	N.A.	N.A.	0.0162	-0.0083
S2-C2-90-16-3	N.A.	N.A.	314.18	297.33	325.13	N.A.	N.A.	0.0183	0.0193	0.0247	-0.0092 (-0.0073)
S2-C2-90-25-1	240.05	236.69	254.37	203.84	231.63	0.0074	0.0083	0.0105	0.0117	0.0156	-0.0110
S2-C2-90-25-2	N.A.	N.A.	251.85	210.57	235.84	N.A.	N.A.	0.0140	0.0147	0.0187	-0.0117
S2-C2-90-25-3	N.A.	N.A.	272.06	256.90	265.32	N.A.	N.A.	0.0117	0.0129	0.0192	-0.0109
S2-G4-80-16-1	201.31	192.89	272.06	217.31	251.00	0.0067	0.0068	0.0167	0.0165	0.0195	-0.0115
S2-G4-80-16-2	N.A.	N.A.	272.06	217.31	252.69	N.A.	N.A.	0.0179	0.0179	0.0219	-0.0139
S2-G4-80-16-3	N.A.	N.A.	289.75	227.42	263.64	N.A.	N.A.	0.0181	0.0181	0.0223	-0.0112
S2-G4-80-25-1	N.A.	N.A.	253.53	210.57	220.68	N.A.	N.A.	0.0141	0.0159	0.0180	-0.0100
S2-G4-80-25-2	N.A.	N.A.	251.00	239.21	231.63	N.A.	N.A.	0.0120	0.0132	0.0172	-0.0102
S2-G4-80-25-3	N.A.	N.A.	267.85	247.64	279.64	N.A.	N.A.	0.0149	0.0152	0.0221	-0.0120 (-0.0074)
S2-G6-80-25-1	N.A.	N.A.	293.12	285.54	329.34	N.A.	N.A.	0.0175	0.0177	0.0309	-0.0169
S2-G6-80-25-2	N.A.	N.A.	289.75	263.64	308.28	N.A.	N.A.	0.0127	0.0133	0.0233	-0.0131
S2-G6-80-25-3	N.A.	N.A.	283.01	259.43	299.86	N.A.	N.A.	0.0142	0.0151	0.0241	-0.0122
S1-G4-80-0-1	195.41	187.83	N.A.	N.A.	222.37	0.0070	0.0086	N.A.	N.A.	0.0161	-0.0103
S1-G4-80-0-2	176.04	149.93	N.A.	N.A.	209.73	0.0049	0.0064	N.A.	N.A.	0.0161	-0.0061
S1-G4-80-0-3	198.78	180.25	N.A.	N.A.	225.74	0.0072	0.0078	N.A.	N.A.	0.0184	-0.0117 (-0.0101)
S1-G4-60-0-1	176.88	130.56	N.A.	N.A.	185.31	0.0043	0.0058	N.A.	N.A.	0.0202	-0.0175
S1-G4-60-0-2	175.20	135.61	N.A.	N.A.	190.36	0.0040	0.0052	N.A.	N.A.	0.0232	-0.0147
S1-G4-60-0-3	163.41	128.87	N.A.	N.A.	181.94	0.0045	0.0070	N.A.	N.A.	0.0234	-0.0124
S1-G4-45-0-1	169.30	90.97	N.A.	N.A.	98.55	0.0044	0.0052	N.A.	N.A.	0.0881	-0.0557
S1-G4-45-0-2	165.09	70.75	N.A.	N.A.	110.34	0.0048	0.0132	N.A.	N.A.	0.1009	-0.0932 (-0.0430)
S1-G4-45-0-3	171.83	105.29	N.A.	N.A.	121.29	0.0050	0.0065	N.A.	N.A.	0.1160	-0.0907 (-0.0711)
S2-C1-90-0-1	163.41	124.66	N.A.	N.A.	145.72	0.0037	0.0051	N.A.	N.A.	0.0115	-0.0114
S2-C1-90-0-2	171.83	154.98	N.A.	N.A.	170.14	0.0045	0.0060	N.A.	N.A.	0.0137	-0.0120
S2-C1-90-0-3	169.30	112.87	N.A.	N.A.	155.83	0.0055	0.0057	N.A.	N.A.	0.0132	-0.0094
S2-C2-90-0-1	215.63	184.46	N.A.	N.A.	230.79	0.0080	0.0103	N.A.	N.A.	0.0178	-0.0113
S2-C2-90-0-2	205.52	191.20	N.A.	N.A.	241.74	0.0077	0.0085	N.A.	N.A.	0.0181	-0.0129
S2-C2-90-0-3	N.A.	N.A.	N.A.	N.A.	249.32	N.A.	N.A.	N.A.	N.A.	0.0228	-0.0132

S2-G4-80-0-1	190.36	181.94	N.A.	N.A.	224.05	0.0086	0.0103	N.A.	N.A.	0.0217	-0.0145
S2-G4-80-0-2	204.68	187.83	N.A.	N.A.	218.16	0.0073	0.0083	N.A.	N.A.	0.0171	-0.0119
S2-G4-80-0-3	192.04	163.41	N.A.	N.A.	213.10	0.0071	0.0082	N.A.	N.A.	0.0183	-0.0114
S2-G6-80-0-1	188.67	178.57	N.A.	N.A.	281.33	0.0069	0.0077	N.A.	N.A.	0.0273	-0.0158
S2-G6-80-0-2	N.A.	N.A.	N.A.	N.A.	303.12	N.A.	N.A.	N.A.	N.A.	0.0296	-0.0096 (-0.0049)

Note: f'_{c1}, ε_{c1}, f'_{c2}, ε_{c2}, f'_{c3}, ε_{c3}, f'_{c4}, ε_{c4}, f'_{cu}, ε_{cu} —— Refer to Fig. 13 for definitions; $\varepsilon_{h,rup}$ —— Hoop rupture strain of the outer FRP tube; The value in bracket —— Hoop strain of the outer FRP tube at the time of failure of strain gauges; N.A. —— Not applicable.